16 Microfabricated Electrochemical Systems

Shuo Kang and Serge G. Lemay

CONTENTS

16.1 INTRODUCTION

The terms *microfabrication* and *micromachining* represent a broad set of techniques for systematically creating solid-state structures on the micro- and nanometer scales. Primarily developed by the semiconductor industry as an enabler for cheaper and more complex microelectronics circuitry, the resulting capabilities have since been exploited throughout most other areas of science and technology. In particular, microfabrication, having first become a workhorse of solid-state physics research, has become increasingly common in a variety of *wet* fields ranging from biophysics and neuroscience to environmental sensing and bioanalytical applications. Lithographic approaches are particularly well matched to the demands of electroanalytical methods due to the latter's emphasis on solid-state electrodes and electrical signals and a growing interest in micro- and nanoscale systems and processes.

Microfabrication techniques offer several broad benefits when compared to alternative methods for fabricating miniaturized electrochemical measurement systems:

- Harnessing the well-developed, systematic fabrication protocols developed in the context of microelectronics leads in principle to highly reproducible results for the size and geometry of nanostructures. This is notoriously difficult to achieve on the nanometer scale using alternative approaches based on more ad hoc protocols.
- This reproducibility in turn greatly facilitates characterization since a battery of tools can be brought to bear on a series of nominally identical structures, even when some of these tools are mutually exclusive and/or destructive to the structures. This is again in contrast

to approaches where each (nanoscale) system is individually realized and thus needs to be separately characterized; in these cases, electrochemical measurements themselves are often the only source of characterization available.
- Once a measurement system is developed, the marginal costs associated with large-scale production become relatively low. To fully appreciate the full extent of this point, note that standard complementary metal-oxide semiconductor (CMOS) technology allows integrating millions of functional components on a mass-produced chip at a cost of only a few dollars.
- For sufficiently complex geometries, there are often no alternative clever *tricks* available and brute-force lithography-based methods are the only option.
- Individual devices can be easily integrated with each other as well as with other electronic and/or fluid handling components. This is particularly relevant in the context of so-called lab-on-a-chip applications. At the extreme limit of integration, a complete measurement system can be integrated on a single chip with a liquid sample as input and digital data as output.

Offsetting these benefits are several complications and limitations introduced by microfabrication:

- Specialized equipment is required that is not available in all laboratories. This is particularly true of the high-end lithography equipment employed in several common approaches for patterning thin-film materials at the submicron level.
- There are experimental issues to which widely accepted solutions have been developed in conventional systems, but that cannot easily be replicated in microfabricated devices. Probably the best example is the difficulty of polishing most microfabricated electrodes, a common procedure with macro- and ultramicroelectrodes (UMEs).
- The extensive processing involved in microfabrication largely precludes working with advanced materials such as single crystals.

These limitations and some of the approaches that have been explored to mitigate them will be the main focus of this chapter, with a particular focus on concrete examples.

We note that the development of microfabricated electrochemical systems over the last 30 years has largely progressed in an evolutionary rather than revolutionary manner. But whereas many of the basic motivations, principles, and approaches have remained relatively unchanged, their realization has become increasingly sophisticated and their performance has continually improved as a result of new insights and more advanced fabrication methods. This is illustrated in Figure 16.1, which contrasts two setups—one early and one recent—for redox-cycling measurements. Figure 16.1a shows a measurement cell based on microfabricated interdigitated electrodes (IDEs) (discussed in Section 16.4.1). The critical dimension of the microfabricated structure, namely, the spacing between the electrodes, was 50 μm. Figure 16.1b shows the corresponding arrangement for a recent nanofluidic thin-layer cell (discussed in Section 16.4.3). Here, the electrode spacing is 50 nm, leading to a thousandfold increase in diffusive fluxes. Both cells allow for convective transport, with the caveat that this requires a more sophisticated polydimethylsiloxane (PDMS) microfluidic interface in the case of the nanodevice.

The present chapter focuses on summarizing the evolution and the current status of microfabrication-based approaches for the realization of electroanalytical systems. In keeping with the general theme of this book, we focus primarily on nanoscale systems where possible. In areas where little work has reached this level of miniaturization, we instead discuss the state of the art at the micrometer scale. We assume that the reader has some familiarity with basic lithography-based fabrication methods and dwell only briefly on the general methods. For a more general introduction, we refer the uninitiated reader to a recent tutorial overview.[1] Here, we instead concentrate on aspects of direct relevance to electrochemical methods or to the specific works being reviewed.

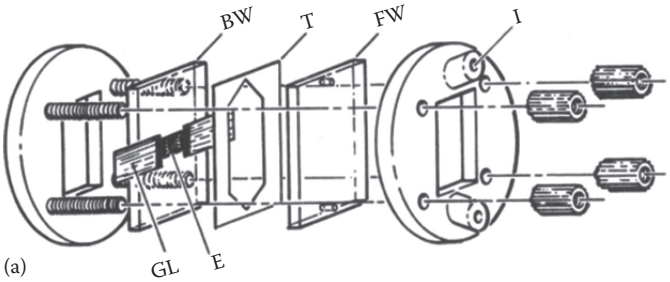

(a)

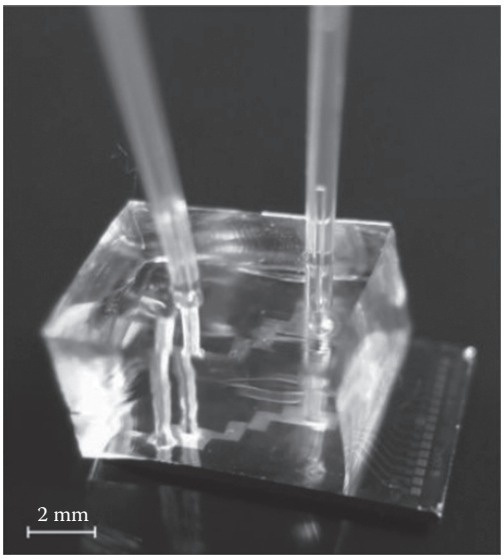

(b)

FIGURE 16.1 (a) Schematic drawing of assembly of IDEs (E) microfabricated on a quartz substrate with electrical contacts (GL) and liquid chamber (T + BW + FW). BW, back window; FW, front window; GL, gold leaf contact; I, injection port; T, Teflon spacer. (Reprinted with permission from Sanderson, D.G. and Anderson, L.B., Filar electrodes—Steady-state currents and spectroelectrochemistry at twin interdigitated electrodes, *Analytical Chemistry*, 1985, 57, 2388–2393. Copyright 1985 American Chemical Society.) (b) Photograph of a microfabricated electrochemical nanofluidic device; the contact pads and wires to individual electrodes are visible on the bottom right. Microfluidic channels molded in the transparent PDMS block allow delivering fluid to the electrochemical device. (From Mathwig, K. and Lemay, S.G., *Micromachines*, 4, 138, 2013.)

The chapter is further organized in order of increasing complexity of the structures being discussed, starting with methods for the fabrication of individual electrodes and concluding with a brief discussion of systems in which electrochemical probes are fully integrated with microelectronics on the same chip.

16.2 ULTRAMICROELECTRODES AND ULTRAMICROELECTRODE ARRAYS

UMEs[2,3] offer several advantageous features compared to their macroscopic counterparts including a true steady-state diffusion-limited current, small IR drops from solution resistance, and short RC response times. Originally aimed at precise measurements of diffusion coefficients, interest in UMEs was further stoked by attempts at probing electroactive species inside brain tissue, which necessitated small, nonperturbing probes.[4,5] Classical methods for fabricating UMEs were largely

based on micrometer-diameter wires that were either selectively insulated or encased in glass micropipettes. These methods were used successfully in producing high-quality monolithic UMEs that were suitable for intra- and extracellular stimulation and recording[6,7]; indeed, similar electrodes are still in use today. It, however, proved more challenging to employ these approaches to fabricate bundles of closely spaced microelectrodes to monitor neural activity at a number of nearby sites simultaneously. In the 1970s, micromachining technology was thus introduced to fabricate arrays of (separately addressable) microelectrodes for both in vitro and in vivo experiments.[8–12] Arrays of identical UMEs connected in parallel can also be beneficial in other applications since faradaic currents at UMEs are relatively small: wiring many electrodes together amplifies the magnitude of the current while retaining the beneficial features of UMEs.[13]

An early work was presented by Thomas et al.[8] who fabricated a miniature microelectrode array to monitor the bioelectric activity of cultured heart cells. A glass coverslip was used as a substrate on which a 200 nm thick nickel film was deposited and then defined by lithography. Afterwards, gold was electroplated onto the nickel pads, and a photoresist layer was coated and patterned to reveal only the gold electrodes. The remaining resist then functioned as a passivation layer. Finally, a glass ring was affixed to the insulated array with bees' wax, creating a culture chamber, and platinum black was electrochemically deposited on the electrodes.

As an example of a miniaturized tool for in vivo neural recordings, a 24-channel microelectrode array fabricated based on thin-film technology was developed by Kuperstein and Whittington.[14] In this work, Mo foil was used as a temporary substrate on which to build structures. KTFR photoresist, Au, and another layer of KTFR resist were deposited and patterned in succession; thereafter, the Mo foil was electrolytically etched away in an aqueous solution of 5% KOH, 5% $K_3Fe(CN)_6$, and 1% liquid Woolite (the latter atypical reagent playing the role of "low foaming, nonionic, water soluble, and alkali resistant surfactant compound"[15]). In this manner, a probe consisting of arrays of Au recording sites sandwiched between two KTFR resist layers was generated, each of the recording site having an area of 120 μm^2 and being separated from neighboring sites by a gap of 85 μm. Finally, platinum black was plated onto the recording sites of the probe.

During the same period, a multicathode polarographic oxygen electrode with several cathodes connected in parallel in a single package was demonstrated by Siu and Cobbold.[16] The device consisted of circular Au cathodes surrounded by a continuous Ag/AgCl anode created with thin-film technology. Electrical contact between the anode and the cathode was maintained via a salt bridge formed by an electrolyte-containing membrane that covered the surface of the electrodes. The membrane also functioned as a protection layer to prevent the electrodes being contaminated in the meantime.

In the following decades, microfabricated UMEs and UME arrays became increasingly widespread, as reviewed by Feeney and Kounaves.[17] An advantage of the added flexibility provided by micromachining started to be exploited by fashioning sets of electrodes from different materials. For example, Glass et al.[18] fabricated a multielement microelectrode array for environmental monitoring including 66 working electrodes on a 2 in. silicon wafer with a variety of electrode materials including Pt, Au, V, Ir, and carbon deposited and defined by separate lithography steps. Different electrode materials displayed somewhat different responses to a given compound in voltammetric measurements, in principle increasing the selectivity compared with using a single electrode material.

In recent years, designs for UMEs and UME arrays continue to evolve. For example, works based on microfabricated diamond UMEs and arrays are increasingly common, motivated by this material's attractive properties as an electrode that include mechanical stability, chemical inertness, low background currents, wide potential window, and resistance to electrode fouling.[19] Individual electrodes fabricated with focused ion beam (FIB)[20] and arrays fabricated with thin-film technology[21,22] were demonstrated.

Instead of exploiting the advantages of a high degree of integration, addressable electrode arrays with each sensing pixel wired via multiplexing circuitry to a potentiostat were developed for sensing

and imaging.[23,24] For instance, a multianalyte microelectrode detection platform capable of discriminating between multiple protein and DNA analytes simultaneously was demonstrated.[25] The electrodes were selectively functionalized with enzymes, antibodies, DNA, and peptide probes using an electrically addressable deposition procedure.

A method for fabricating 3D electrode structures was demonstrated by Sanchez-Molas et al.[26] to effectively extend the electrode surface area. In this case, the motivation for creating such structures originated from biofilm-based microbial fuel cell applications. High-aspect-ratio micropillars were formed by micromachining a silicon wafer with deep reactive ion etching (DRIE), the radius of the pillars being 5–10 μm with a separation of 20–100 μm in between and a height of 5–125 μm. A multilayer of Ti/Ni/Au was sputtered onto the structure surface to ensure the metallization of both the vertical walls and the bottom surface between the pillars.

16.3 NANOELECTRODES AND NANOELECTRODE ARRAYS

In recent years, considerable attention has shifted to nanoscale electrodes (as already discussed in Chapter 15) and integrated systems.[27–30] With this further downscaling, the intrinsic advantages of UMEs such as small ohmic drops and fast response times are further amplified. Mass transport also becomes so efficient that even fast electrochemical reactions become increasingly limited by the rate of heterogeneous electron transfer, allowing ultrafast electron-transfer kinetics to be studied. Furthermore, because the electrode size becomes comparable to the thickness of the electrical double layer and to the size of macromolecular analytes, new mass-transport phenomena have been predicted and new analytical applications can be considered, respectively.[31]

The challenge of fabricating and characterizing nanometer-scale electrodes is, however, substantial compared to microelectrodes. In particular, the ability to project a sharp image of a small feature onto the substrate in photolithography is limited by the wavelength of the light that is used and the ability of the reduction lens system to capture enough diffraction orders from the illuminated mask.[32] Even though the most advanced optical immersion lithography tools currently allow features of ~40 nm to be realized in integrated-circuit (IC) processing, the necessary equipment is very specialized and mostly targeted at semiconductor research and manufacturing. Most readily accessible optical-lithography equipment in universities and research laboratories instead has a much more modest practical resolution of ~1 μm. Consequently, a broad range of alternative approaches has been explored for micromachining nanoscale electrochemical systems. These include lithographic methods with higher resolution, such as e-beam, nanoimprint, and nanosphere lithography, electrode materials prepared by bottom-up approaches, and a number of one-of-a-kind solutions for creating specific structures.

16.3.1 Tip-Based Nanoelectrodes

The bulk of the approaches employed for pioneering studies of nanoelectrodes was evolved from methods for preparing UMEs and/or tips for scanning electrochemical microscopy (SECM).[33,34] Broadly speaking, these methods rely on preparing sharp conducting wires or tips and covering all but the apex with an insulating material, including wax,[35–37] polyimide,[38] electrophoretic paint,[39–46] or glass.[47–53] Because the electrodes are prepared individually, these approaches have historically tended to exhibit limited reproducibility. This prompted some authors to explore micromachining-based approaches for fabricating tip-based electrodes.

Thiébaud et al.[54] developed tip-like electrodes based on a fully controlled lithographic process. Atomically faceted, 47 μm high tips were carved out of a <100> silicon wafer by anisotropic etching in KOH. The silicon was then successively coated with thin films of silicon dioxide, platinum, and silicon nitride. Following a final lithography step, the nitride was etched away from the apex of the tip to leave a Pt tip exposed with a height as small as 2 μm. In an alternative hybrid approach, Qiao et al.[55] first etched tungsten wires to yield tips with diameters below 100 nm and insulated these

wires using electrophoretic paint. The FIB technique was then employed to selectively remove the insulating paint and sculpt the Pt tip apex to the desired shape. Tips with dimensions 100–1000 nm were realized in this manner.

Despite their potential benefits in terms of control and characterization, however, these approaches have not proven competitive compared to the more accessible classic approaches for fabricating tip electrodes.

16.3.2 Top-Down Fabrication of Nanoelectrodes

Despite the limited resolution of optical lithography, this method has been employed to create nanoelectrodes by incorporating nonstandard microfabrication steps. For example, Menke et al.[56] combined top-down lithography and electrodeposition to generate band electrodes with a width of 40–50 nm in a process coined lithographically patterned nanowire electrodeposition (LPNE). The process flow for the fabrication is shown in Figure 16.2. By undercutting nickel bands that were covered with a layer of photoresist, a trench was formed, and nanowires were grown by electrodeposition in the trench along the edge of the nickel bands. The height of the nanowires was determined by the thickness of the nickel bands and the width by controlling the deposition process. A hydrogen gas detector consisting of Pd nanowires fabricated using this method was demonstrated,[57] and the method was also improved by adding further processing steps to fabricate arrays of nanowires.[58] To overcome the restrictions imposed on the array density by the limited resolution of photolithography, repeated alternating deposition of nanowire electrodes and nickel bands was performed, the array being generated when all the nickel bands were simultaneously released in a subsequent step.

Another method for beating the resolution limitations of optical lithography was demonstrated by Heo et al.[59] who derived a carbon linear nanoelectrode array from optical-lithography-defined polymer microstructures. Photosensitive polymer SU-8 was coated and patterned on a 6 in. passivated silicon wafer and subsequently pyrolyzed at 900°C in vacuum. During the pyrolysis process, the SU-8 was carbonized and the dimension of the structures shrank by approximately 60% in width and 90% in height, as shown in the scanning electron microscope (SEM) images of Figure 16.3.

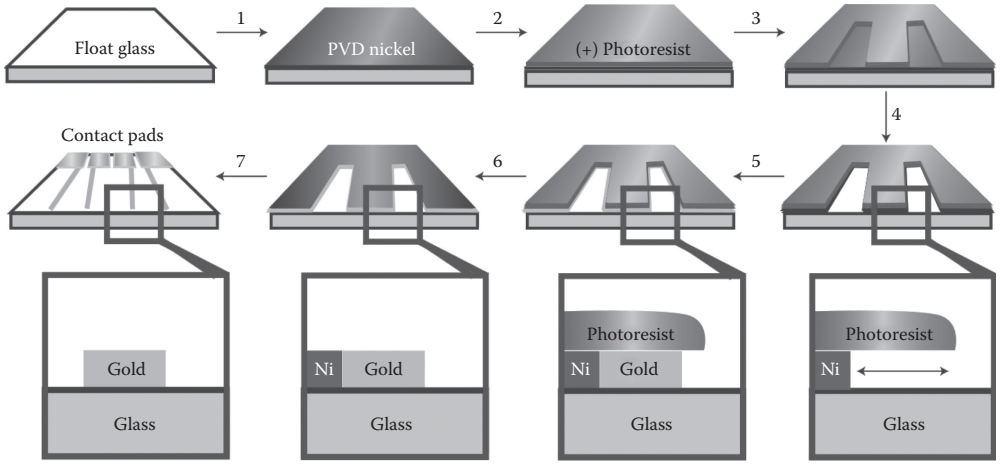

FIGURE 16.2 Process flow for lithographically patterned nanowire electrodeposition. (Reprinted by permission from Macmillan Publishers Ltd. *Nature Materials*, Menke, E.J., Thompson, M.A., Xiang, C., Yang, L.C., and Penner, R.M, Lithographically patterned nanowire electrodeposition, 5, 914–916, 2006. Copyright 2006.)

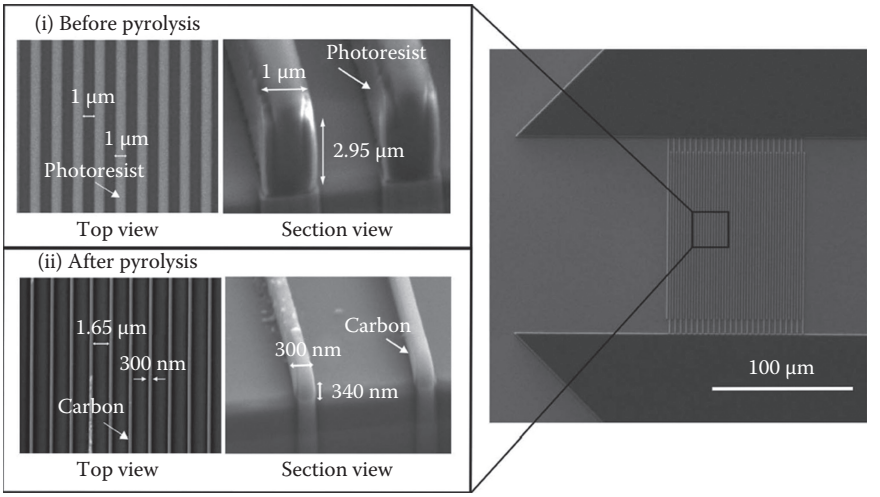

FIGURE 16.3 SEM images of nanoscale carbon electrodes pyrolyzed from SU-8 microstructures. (From Heo, J.I. et al., *J. Electrochem. Soc.*, 158, J76, 2011. By permission of The Electrochemical Society.)

The pyrolysis process was reported to be controllable such that the final dimensions of the carbon electrodes were predictable.

Despite these successes of optical-lithography-based approaches, patterning of nanoscale structures is more typically carried out using a workhorse of nanoscience and nanotechnology, electron-beam lithography (EBL). This tool, which was developed in the early 1970s,[60] employs a focused beam of electrons to write arbitrary 2D patterns on a surface covered with an electron-sensitive resist. Apart from these differences, the whole range of thin-film technologies can be combined with EBL with only minor adjustments to the processes compared with optical lithography. It is a serial patterning technology rather than simultaneous patterning as in optical lithography, rendering the process more time consuming and therefore costly, but this is compensated by the feature that resolutions in the range 10–100 nm can be achieved with EBL, depending on the specific equipment employed.

A variety of nanoelectrochemical systems fabricated with EBL has been demonstrated.[61–67] As an early example, Niwa et al.[68] reported electrode arrays with submicron dimensions. Electrochemical analysis based on EBL-generated individual Au nanowires was reported by Dawson et al.[66] A catalytic signal from fewer than 50 enzyme molecules immobilized on an EBL-patterned nanoelectrode was also reported.[64]

Another technique used to pattern nanostructures from thin films is FIB milling, which operates in a fashion analogous to an SEM except that a finely focused beam of ions (usually gallium) is used instead of electrons. A FIB can be operated at low beam currents for imaging or high beam currents for site-specific sputtering or milling. A disadvantage is that this is also a serial method, individual structures needing to be prepared separately. One way to use FIB to generate electrodes is to first deposit a metal and an insulating layer and then drill holes through the insulating layer to uncover the electrodes.[69–71] With this method, recessed electrodes located at the bottom of truncated conical pores result.[69]

Alternatively, it is also possible to generate electrodes by first creating nanoscale holes through thin insulating membranes and then filling these holes from one side of the membrane with a conducting material to create electrode structures on the other side of the membrane. This approach is conceptually descended from earlier protocols to create nanoelectrode ensembles by depositing metal in a porous host membrane such as polycarbonate (PC).[72] Besides FIB milling, a focused electron beam from a transmission electron microscope can also be used to drill individual

nanopores.[73–76] An advantage of the latter approach is that a nanometer-resolution image of each nanopore can be simultaneously obtained. Since the diameter of the finished electrodes is dictated by that of the original pores, this provides an independent characterization of the electrode size. Krapf et al. demonstrated electrodes as small as 2 nm using this approach.[75]

High-throughput, high-resolution lithographic methods have also been developed. Nanoimprint lithography[77] creates patterns by mechanical deformation of a so-called imprint resist that typically consists of a monomer or polymer formulation cured by heat or UV light during the imprinting. A master stamp provides the pattern to be imprinted; while this stamp must first be created using another lithography method, it is not significantly degraded by the imprinting process and can be reused over an extended period of time. A challenge of this technique is that the process is strongly dependent upon the pressure, temperature, time control, and even the geometry of the stamp. Nonetheless, electrode arrays created by nanoimprint lithography have been demonstrated and suggested for low-cost sensor production.[62,78,79]

Another, much simpler and low-cost alternative for fabricating electrodes is nanosphere lithography,[80–84] in which self-assembled monolayers of spheres are used as masks instead of selectively exposed polymer layers. For example, Valsesia et al.[81] spin-coated polystyrene beads with a diameter of 500–1000 nm onto an Au-coated substrate, forming a monolayer of hexagonally packed beads whose surface coverage could be adjusted by tuning the spin-coating acceleration. With a treatment in oxygen plasma, the size of the beads was reduced by half. Afterwards, a layer of silicon oxide was deposited and lifted off by mechanically removing the beads in an ultrasonic bath. The resulting recessed Au spots with dimensions in the range of 50–120 nm and surrounded by silicon oxide were then used as templates to electrochemically grow polypyrrole nanopillar electrodes.

Diamond nanoelectrode ensembles and arrays were created by Hees et al.[83] using nanosphere lithography and EBL, respectively. In the first approach, a substrate coated with a trimethylboron-doped nanocrystalline diamond (NCD) film was immersed in an ultrasonic bath with suspended SiO_2 spheres having a radius of 500 nm and a concentration of ~10^{-7} cm^{-3}. The spheres adhered to the surface in a random pattern. An insulating NCD layer was then deposited onto the surface and lifted off by removing the SiO_2 beads with hydrofluoric acid (HF), creating recessed boron-doped diamond electrodes surrounded by an insulating NCD layer. The radius of the electrodes was about 175 nm and the average distance between them was 10 μm. In the second approach, all the process steps were identical except that EBL-patterned plasma-enhanced chemical vapor deposition (PECVD) SiO_2 was used instead of SiO_2 beads for lifting off the passivation NCD film. Electrode arrays following regular hexagonal patterns were formed in this manner. SEM images of the electrodes and arrays fabricated with both methods are shown in Figure 16.4. Based on these arrays, changes in electron-transfer rates were observed to change when switching the NCD surface termination from hydrogen to oxygen; this subtle effect was not observed based on macroscopic planar diamond electrodes.

16.3.3 Nanowire-Based Nanoelectrodes

In the approaches described so far, micro- and nanoscale electrodes were created by patterning thin conductive and/or insulating films into the desired geometry. An alternative bottom-up approach is to first synthesize electrode materials with nanoscopic dimensions, then to interface these materials to external interconnects to enable electrochemical measurements. Wire-shaped objects with nanometer-scale diameters and micrometer-scale lengths are particularly well suited for this approach: the long lengths make it relatively straightforward to pattern interconnects using relatively low-resolution lithography, while the small diameters mean that the materials effectively function as nanoscale band electrodes.[85]

This approach is perhaps best illustrated by the use of single-wall carbon nanotubes (SWNTs) as electrode materials. SWNTs are cylindrically shaped carbon macromolecules. They can be readily deposited on a substrate or, often preferably for device applications, grown by CVD from catalyst

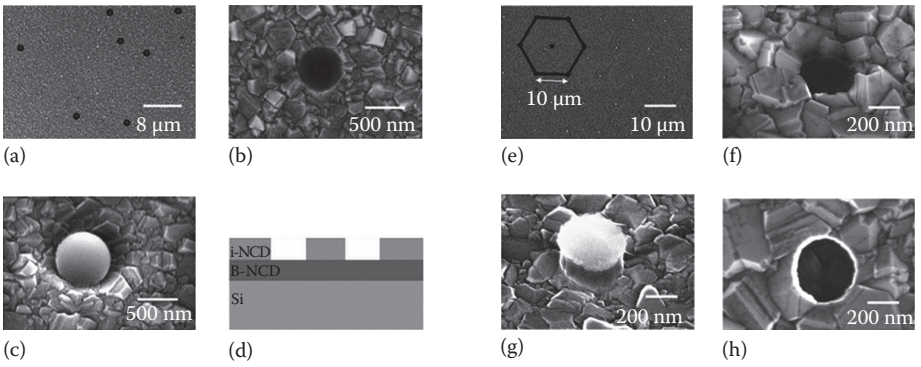

FIGURE 16.4 (a through d) SEM images and schematic cross section of diamond nanoelectrode ensembles fabricated with nanosphere lithography and (e through h) arrays fabricated with EBL. (a) Overview of randomly distributed electrodes. (b) SiO_2 sphere after deposition of insulating diamond. (c) Final boron-doped NCD electrode after removal of SiO_2. (d) Schematic cross section of fabricated electrodes. (e) Overview of electrodes distributed in hexagonal pattern. (f) Structured SiO_2 island on boron-doped NCD layer. (g) Insulating diamond grown around SiO_2. (h) Final recessed diamond electrode. (Reprinted with permission from Hees, J., Hoffmann, R., Kriele, A. et al., Nanocrystalline diamond nanoelectrode arrays and ensembles, *ACS Nano*, 2011, 5, 3339–3346. Copyright 2011 American Chemical Society.)

particles that can be deposited according to lithographically defined patterns on a solid substrate. The diameter and length distribution varies substantially depending on the growth method, but diameters of 1–3 nm and lengths of a few micrometers are typical and readily achievable. In a common approach, the nanotubes are first deposited or grown on the substrate, metal interconnects are added to make contact to one or more nanotube, and a passivation layer is deposited and patterned so as to cover the electrodes but leave (part of) the nanotubes exposed. Since the sidewalls are electrochemically active,[86] each individual nanotube functions as a band nanoelectrode. But because the geometry of the nanotube(s) and passivation can be controlled, a greater range of electrode geometries can also be created. In particular, Dumitrescu et al.[87,88] showed that a relatively sparse network of randomly oriented, interconnected SWNTs can effectively function as a 2D array of nanoelectrodes with overlapping diffusion fields: the total diffusion-limited current at a disk-shaped network electrode was shown to be equivalent to that to an UME of the same shape and size, but the current density at the surface of the SWNTs was much higher than at the corresponding UME. Alternatively, exposing only the sidewall of an individual SWNT leads to a near-ideal cylindrical electrode with a radius of ~1 nm.[89] Finally, exposing only the end allows forming a point-like electrode with the same radius.[90] In cases where a different electrode material is needed, it was also shown that SWNTs can also be modified with metal nanoparticles by electrodeposition. In these applications, the SWNTs serve both as a template for deposition and as interconnects between the nanoparticles and external wiring. Paralleling the work on bare SWNTs, such deposition has been employed to create 2D (networks), 1D (wires), and 0D (single particles) nanoparticle electrodes.[90–92]

Similar approaches have been applied to a broad range of other 1D nanostructures. For example, Dawson et al.[93] demonstrated electrodes based on Au nanowires with a rectangular (~210 × 250 nm) cross section created by nanoskiving.[94] This method is based on first forming a block consisting of thick epoxy layers separated by an Au film. Thin slices of this block are then sectioned off in a plane perpendicular to the layers. Finally, the epoxy is dissolved, leaving only Au nanowires available for contacting via lithographically defined external wires. Other examples of individual nanowires that have been investigated as electrochemical nanoelectrodes include multiwalled carbon nanotubes,[95] carbon nanofibers,[96] vanadium oxide nanowires and Si/amorphous–Si core/shell nanowires,[97] mesoporous ZnO nanofibers,[98] and platinum nanowires prepared by laser pulling.[99]

16.3.4 Electrodes for Electrochemical Atomic Force Microscopy

Another area where microfabricated electrodes have played a significant role is in the preparation of advanced scanning probes, in particular modified cantilevers for atomic force microscopy (AFM) with electrochemical functionality. In AFM, a sharp point mounted at the end of a flexible cantilever is scanned along a surface, and the deflection of the cantilever or its resonance amplitude is used as feedback signal to control the height of the cantilever. Subnanometer resolution can be achieved in the height direction, while the lateral resolution is largely determined by the sharpness of the tip being employed; micromachining is commonly used for manufacturing sharp, reproducible cantilever and tip structures. Several authors have explored the possibility of modifying cantilevers to incorporate one or more electrodes in AFM tips.[100–104] In this way, local electrochemical measurements can be performed while AFM feedback is employed for imaging and tip positioning.

As an early example, silicon nitride cantilevers were modified by patterning a ring electrode immediately around the apex of the AFM tip.[100,101] This was achieved by coating the original silicon nitride cantilever with Au and an insulating silicon nitride layer, then milling the apex of the tip to create a sharp silicon nitride point (made from the original cantilever material) surrounded by a ring of exposed gold. The sharp nitride tip provides imaging capabilities and stability comparable to those of the original cantilever, while the ring electrode, contacted via the Au film, permits electrochemical measurements. In an alternative approach, Burt et al.[102] attached a metal nanowire to the end of an AFM tip. The wire, which was fabricated by coating an SWNT template, was insulated and then cut to create an Au disk nanoelectrode. This geometry results in a flat tip that reduces AFM resolution but has the benefit of allowing SECM measurements with simultaneous AFM imaging. More recent developments in this area include needle-shaped, individually addressable dual tips[103] and insulating diamond tips with integrated boron-doped diamond electrodes.[104] In most approaches to AFM tip modification, the FIB technique has been the method of choice to precisely sculpt the complex geometry of the critical region near and at the apex of the tip.

16.4 REDOX-CYCLING AND GENERATOR–COLLECTOR ELECTRODES

In the micro- and nanoelectrode arrays discussed earlier, the motivation for creating a multielectrode system is most often to amplify the faradaic current while retaining the beneficial properties of the individual miniature electrodes. The constituting electrodes thus function essentially independent of each other. Redox-cycling and generator–collector approaches instead exploit the interplay between redox reactions taking place at two or more electrodes. Establishing an effective coupling between electrodes requires careful control of electrode geometry and placement, a challenge that plays to the strengths of microfabrication techniques.

In generator–collector systems, the product of a reaction taking place at a generator electrode is detected at a second, so-called collector electrode. A natural figure of merit is the collection efficiency, which corresponds to the fraction of generated molecules that are collected. In redox cycling, both electrodes instead share both roles of generator and collector, as chemically reversible species are repeatedly reduced at one electrode and oxidized at the other. The geometries required for efficient redox cycling tend to be more restrictive than for generation–collection, since in this case the collection efficiency should be high for both halves of the cycle. A common figure of merit in redox cycling is the amplification factor, which essentially corresponds to the average number of times that each molecule is cycled before it exits the detection domain. Consistent with intuition, both the collection efficiency and the amplification factor tend to increase as the distance between the electrodes is reduced due to more effective mass transport.[3] Generator–collector and redox-cycling systems are thus natural candidates for miniaturization to the nanoscale.

At this time, three main classes of devices are undergoing the most extensive development toward nanoscale applications: IDEs,[59,68,105–111,185] recessed ring–disk (RRD) electrodes,[84,112–117] and nanogaps,[118–130] as summarized in Figure 16.5.

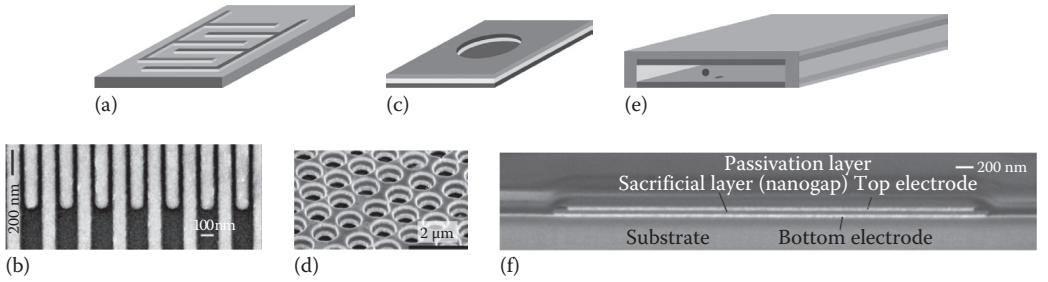

FIGURE 16.5 (a, c, e) Schematic drawings and (b, d, f) SEM images of IDEs, RRD electrodes, and nanogaps, respectively. (b) Top view of IDEs. (Reprinted from Ueno, K., Hayashida, M., Ye, J. and Misawa, H. Fabrication and electrochemical characterization of interdigitated nanoelectrode arrays, *Electrochemistry Communications*, 7, 161–165, Copyright 2005, with permission from Elsevier.) (d) View from an angle of an RRD electrode array. (Reprinted with permission from Ma, C., Contento, N.M., Gibson, L.R., 2nd, and Bohn, P.W., Recessed ring-disk nanoelectrode arrays integrated in nanofluidic structures for selective electrochemical detection, *Analytical Chemistry*, 2013, 85, 9882–9888. Copyright 2013 American Chemical Society.) (f) View from an angle of the cross-section of a nanogap. (Reprinted with permission from Kang, S., Nieuwenhuis, A.F., Mathwig, K., Mampallil, D., and Lemay, S.G., Electrochemical single-molecule detection in aqueous solution using self-aligned nanogap transducers, *ACS Nano*, 2013, 7, 10931–10937. Copyright 2013 American Chemical Society.)

16.4.1 Interdigitated Electrodes

The most widely reported redox-cycling device configuration, illustrated in Figure 16.5a and b, is the IDE or, equivalently, interdigitated array (IDA).[59,68,105–111,185] It consists of two coplanar, interpenetrating comb-shaped electrodes. Because the two electrodes can be realized simultaneously by patterning a single layer of conducting material, this geometry is conceptually straightforward from a fabrication point of view. By the same token, the smallest achievable electrode spacing is set by the lateral resolution of the lithographic process employed. IDEs with electrode spacing ranging from microns down to tens of nanometers were correspondingly demonstrated using optical,[107,131,132] e-beam,[61] and nanoimprint lithography.[78,79] Amplification factors up to ~10^2 are typically reported with these structures.

In a pioneering article, Sanderson and Anderson[105] reported coplanar IDEs fabricated by depositing and defining a layer of Au (1000–2000 Å) with 200–400 Å Cr as an adhesion layer on a quartz substrate with photolithography and subsequent wet etching. Each electrode was 0.5 cm long and 50 μm wide, separated from the adjacent electrodes by a gap of 50 μm. Two strips of gold leaves were placed onto the metal pads to make electrical contacts. A liquid cell was formed by clamping the quartz substrate and a Teflon spacer between two quartz windows with quick-tightened screws, as indicated in the schematic drawing shown in Figure 16.1a; amplification of the faradaic current by redox cycling was successfully observed in this system. Several years later, further downscaled electrode arrays with feature sizes ranging from 0.75 to 10 μm fabricated using both optical and EBL were reported by Niwa et al.[68] A layer of spin-on glass was coated onto wafers as passivation, and the electrodes and contact pads were uncovered by etching through this passivation layer using reactive ion etching (RIE).

Besides electrode spacing, the signal amplification provided by IDEs also depends on the width and the aspect ratio of the electrodes.[133] Electrodes with a relatively large height-to-width ratio were shown to generate a higher amplification factor than planar electrodes, as the short linear diffusion path created between the electrode sidewalls increases the diffusive flux. Dam et al.[108] reported intentionally vertically faced IDEs. Trenches were first created by DRIE on a silicon wafer, after which the electrode material (Pt together with a Ti adhesion layer) was deposited onto the

sidewalls of the trenches by evaporation under a 45° incident angle. While the minimum separation between the electrodes was only 2 μm, a relatively high amplification factor of 60–70 was nonetheless achieved with this device because of the advantageous 3D geometry.

Another method introduced by Goluch et al.[109] for achieving higher amplification factors is to encase an IDE inside a fluidic channel, thus minimizing the loss of analyte molecules to the bulk solution above the IDE and increasing the average number of cycles undergone per molecule. Calculations indicate that the increase becomes most pronounced once the height of the channel becomes comparable to or smaller than the lateral electrode finger spacing. By embedding an IDE with a finger spacing of 250 nm in a series of parallel, 75 nm tall fluidic channels, an amplification factor of 110 was obtained. This was used to show that the confined IDE was capable of detecting paracetamol, a chemically reversible species, in the presence of a large excess of (irreversible) ascorbic acid. More recently, Heo et al. reported an amplification factor of 1100 in devices combining vertical face and confinement in a microchannel.[133]

At a higher degree of parallelization (albeit not of miniaturization), an addressable IDA fabricated on a single glass substrate and consisting of 32 rows and 32 columns of electrodes forming 1024 addressable sensing pixels was reported by Ino et al.[110,111] The electrodes were defined by sputtered Ti/Pt and the gap between the fingers was 12 μm; each sensing pixel was located at the bottom of a microwell that was formed by photoresist SU-8 and had a dimension of $100 \times 100 \times 7$ μm. Redox signals at each of the 1024 pixels could be acquired within 1 min, based on which a 2D map of the distributions of electrochemical species could be obtained.

16.4.2 Recessed Ring–Disk Electrodes and Arrays

An alternative to the IDE is the coplanar ring–disk electrode, which consists of a central disk-shaped electrode surrounded by a second, ring-shaped electrode.[134–136] A further refinement of this structure that is particularly suitable for microfabrication is the RRD electrode,[84,112–117] (Figure 16.5c and d), in which the two electrodes are placed on different planes. That is, a disk-shaped electrode forms the bottom of a recessed pit, while the ring electrode is located at the rim, also forming part of the sidewalls of the pit. Most such devices are fabricated by etching cylindrical cavities through the first two layers of a metal/insulator/metal stack, the two metal layers thus becoming the electrodes. An important advantage of this approach compared to IDEs is that the size of the gap between the two electrodes is determined by the thickness of the insulating layer, which does not depend on the resolution of the lithographic method employed and which can be straightforwardly controlled down to nanometer resolution.

A theoretical analysis focusing on the current collection efficiency and the transient response for this device geometry was provided by Menshykau et al.[115,116] It was concluded, with support from some experiments, that, in the operation mode where the disk acted as generator electrode and the ring as collector electrode, the current collecting efficiency, which depends on the recess depth and size of the collector ring, could reach 90%.

An interesting work in which RRD electrodes were characterized by both cyclic voltammetry and SECM was provided by Neugebauer et al.[114] Structures with a vertical space between the bottom and rim electrodes of about 200 nm and ring-electrode diameters varying between 200 and 800 nm were created with nanosphere lithography. Electrochemical activity images of single RRD electrodes in good agreement with the ring dimensions were captured, and it was demonstrated how the potential of the unbiased top electrode was influenced by the ratio of the oxidized and reduced form of the redox couples.

In a recent proof of concept for sensor applications, Ma et al.[84,117] reported an RRD electrode array in which the distance between the two electrodes was ~100 nm. Cavities were created with nanosphere lithography through deposited layers of $Au/SiN_x/Au/SiO_2$. The cavities had a radius of about 230 nm, as defined by the size of the polystyrene spheres; an SEM image of the array is demonstrated in Figure 16.5d. The collection efficiency was 98%. The arrays were also confined in

a nanochannel; as a result, the detection selectivity for $Ru(NH_3)_6^{3+}$ in the presence of ascorbic acid was increased by a factor of 7 compared to an array in the absence of confinement.

16.4.3 Nanogaps

Collection efficiency is further improved in a nanogap consisting of two parallel micrometric metal electrodes separated by a thin liquid layer,[118–130] as illustrated in Figure 16.5e and f. Conceptually, this configuration represents a direct downscaling of classic thin-layer cells. But whereas thin-layer cells with micron-scale spacing can be fabricated simply by sandwiching a thin spacer material between two flat electrodes, microfabrication mostly relies on a so-called sacrificial layer approach. A bottom electrode, a sacrificial layer made of a different material, and a top electrode are deposited and patterned on top of each other and passivated with an insulating layer. The resulting structure is illustrated in Figure 16.5f, which shows an SEM image of the cross section of a nanogap device from the authors' laboratory. At least one access hole is then opened through the insulating layer to make contact to the sacrificial layer. In a final step, the sacrificial layer is selectively etched away via the access hole(s) using a wet or isotropic dry etch, leaving a thin-layer cell structure with an electrode spacing determined by the thickness of the sacrificial layer before its removal. The nanogap geometry thus shares with RRDs the benefit that the electrode spacing is set by the thickness of a thin film, which can be accurately controlled, rather than by the resolution of the lithographic method employed. Indeed, nanogaps with spacing 40–65 nm have been demonstrated using micron-resolution optical lithography.[122,125,127] A potential pitfall of this geometry is that any residual strain in the top electrode can cause it to deform slightly; because of the small spacing between the electrodes, even minor buckling can result in a significant relative change in the electrode spacing. This problem was encountered in some early designs in which the electrodes had a square geometry,[118] but was later alleviated through the use of a thin rectangular electrodes[120] or judicious choices of materials.[122,125]

Because of the confined geometry of nanogap devices, the collection efficiency can in certain cases approach 100%, corresponding to a lower bound of ~10^4 for the amplification factor.[120] Largely thanks to this high degree of amplification, the detection of single molecules by redox-cycling electrochemistry was realized in nanogap devices.[123,127] The ability to form arrays of separately addressable nanogap detectors was further exploited in a chip-based recording system enabling in vitro measurements of individual neurotransmitter release events from neurons cultured directly on the chip.[137]

A strategy for further downscaling nanogaps to the sub–10 nm range was demonstrated by McCarty et al.[130] who employed a combination of optical and molecular lithography to minimize the gap size. In their approach, a single- or multilayered molecular film was grown selectively on a first electrode followed by the deposition and patterning of a second electrode, so that the space between the two electrodes was controlled by the thickness of the molecular resist. This molecular layer thus fulfilled the function of sacrificial layer described earlier. The resulting nanogaps took the form of 2 μm long, 50 nm deep crevices between the two electrodes. Gap sizes as small as 4 nm were reported and successfully employed in redox-cycling experiments. The crevice geometry is open to bulk solution in a manner reminiscent of IDEs, for which these devices could provide a higher-performance substitute; the formation of sealed channel structures with higher collection efficiencies can also be envisioned with additional processing steps.

An alternative strategy for further downscaling nanogaps is to decrease the spacing between the electrodes by controlled electrodeposition of additional material on the electrode surfaces.[124] This approach has been employed extensively to create closely separated electrodes, in particular with the aim of measuring the electronic properties of molecules trapped between the electrodes.[138–140] These applications, however, tend to focus on sharp, point-like electrodes that lead to low collection efficiencies. Applying it to parallel planar electrodes would require electrodeposition under

conditions in which mass transport is not limiting in order to achieve a uniform decrease of the electrode spacing. To our knowledge, this has not been realized to date, however.

16.5 ELECTROCHEMISTRY AND MICROFLUIDIC INTEGRATION

Microfluidic systems,[141–143] also referred to as *lab-on-chip* or *micro-total-analysis systems*, consist of fluid handling elements such as valves, mixers, and pumps integrated on a microchip. In general, such miniaturized platforms offer several advantages including the ability to analyze small-volume samples, reduction in reagent consumption and a consequent reduction in the amount of waste to be disposed, and increased speed of analysis as well as potential for parallelization. Electrochemical detection is well suited for these applications as it is more readily integrated with fluidic elements than, for example, optical systems. Indeed, numerous integrated microfluidic electrochemical analytical systems have been reported in the last decade.[144–154]

In the early stages of development, the use of relatively complex silicon- and glass-based micromachining technology developed for ICs was explored to fabricate microfluidic chips.[143] More recently, the focus has shifted toward simpler techniques, micro-/nanofluidic channels being created directly by lithography or molding using low-cost polymers, such as PC,[155] PDMS,[145,156,157] olefin copolymer (COC),[158] and SU-8. [159,160] Among these materials, PDMS has been the most employed for its gas permeability, deformability, and ability to quickly produce prototype devices. It, however, has important drawbacks including in particular analyte absorption and low solvent resistance. COC is a popular alternative for environmental lab-on-a-chip applications due to its high chemical resistance and minimal water adsorption. SU-8, a form of photoresist, is available in a wide range of viscosities, making it suitable to form thick layers and high-aspect-ratio structures. It can be directly spin-coated onto substrates and patterned lithographically, making it particularly convenient for integration with electronic components. Depending on the choice of materials, either the microfluidics are fabricated directly onto a substrate on which electrochemical components have already been defined or the fluidic and electrochemical structures are formed on independent substrates that are bonded together afterwards.

In vitro experiments on living cells have benefited directly from fluidic integration. As discussed in Section 16.2, early approaches relied on glass rings or pierced petri dishes being glued onto electrode substrates to create culture chambers. It is now instead relatively straightforward to build arrays of independent chambers addressable with individual electrodes. For instance, a microwell device fabricated with SU-8 and PDMS for targeting single cells to detect quantal exocytosis—the burst release of intracellular transmitter molecules—was reported by Liu et al.[161] Transparent nitrogen-doped diamond-like-carbon (DLC:N)/indium-tin-oxide (ITO) films were defined on glass slides using photolithography and thin-film etching as electrodes in order to allow visualization of cells immobilized on the electrodes using a conventional inverted microscope. DLC:N was reported to promote cell adhesion and to exhibit good electrochemical properties. SU-8 was then coated and patterned on the slides to form microwells as well as to insulate inactive areas of the conductive film, following which a poly(ethylene glycol) film was grafted to the surface of the SU-8 to inhibit protein adsorption and cell adhesion. Finally, a PDMS gasket was cut and bonded to the substrate to confine a drop of solution containing cells to the middle of the device where 40 working electrodes were located. Single cells were targeted to the electrodes by functionalizing the electrodes with poly(L-lysine). Amperometric responses from individual cells could be recorded unambiguously without interference from nearby extraneous cells, and multiple recordings from the same electrode demonstrated that the device can be cleaned and reused without significant degradation of performance. This showed the potential of this platform as an alternative to carbon-fiber microelectrodes, which are extensively used to study quantal exocytosis of electroactive transmitters, with the additional advantage of increased throughput.

As another example, a disposable polymer-based protein immunosensor was demonstrated by Zou et al.[158] Images, a schematic sketch, and the fabrication process of the device are illustrated in

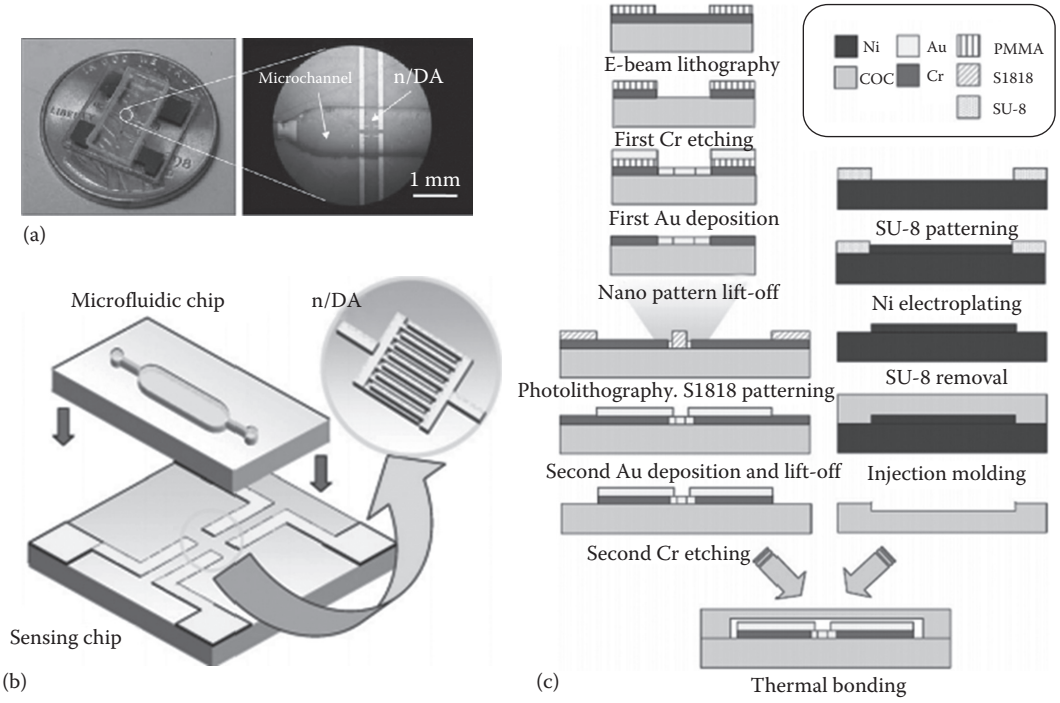

FIGURE 16.6 (a) Optical images, (b) schematic sketch of assembly, and (c) fabrication process for a microfluidic protein immunosensor based on nanoscale IDEs. (Reprinted from *Sens. Actuators A*, 136, Zou, Z.W., Kai, J.H., Rust, M.J., Han, J., and Ahn, C.H., Functionalized nano interdigitated electrodes arrays on polymer with integrated microfluidics for direct bio-affinity sensing using impedimetric measurement, 518–526, Copyright 2006, with permission from Elsevier.)

Figure 16.6. A 3 in. blank cyclic COC wafer with an ultrasmooth surface prepared by plastic injection molding was used as substrate. A gold IDE and contact pads were defined with e-beam lithography and lift-off after the COC wafer was coated with 10 nm Cr layer to render it compatible with lithography. Microfluidic channels were also fabricated in a second COC substrate using the same technique, except that here a Ni mold defined by a combination of lithography and electroplating was used, as shown in the right column of Figure 16.6c. After drilling holes for fluidic connections in the microfluidic chip using a microdrill and growing a self-assembled monolayer of alkanethiols on the gold electrode surfaces, the two substrates were thermally bonded, generating a reaction chamber with a volume of 0.2 μL.

An example of a higher level of multifunctional integration was reported by Ferguson et al.[162] who combined in a microfluidic electrochemical DNA sensor the functionalities of polymerase chain reaction (PCR), single-stranded DNA generation, and sequence-specific electrochemical detection. The architecture and fabrication process of the device are shown in Figure 16.7. The detection system incorporated counter, (quasi-) reference, and working electrodes that were defined by photolithography and lift-off. DNA probes were immobilized on the gold working electrodes via thiol chemistry. In parallel, a liquid chamber was fabricated by bonding a glass chip to a UV–ozone-treated PDMS sheet in which fluidic channels had been cut, and fluidic vias were generated by drilling through the glass chip with a mill equipped with a diamond bit. The exposed side of the PDMS was then bonded to the chip to complete the integration. During use, liquid was pumped into the chamber through eyelets affixed to the vias with epoxy. Comparing with traditional methods, this disposable device was argued to minimize both the sample loss and the likelihood of contamination as the fluid pathways were contained within a sterile system.

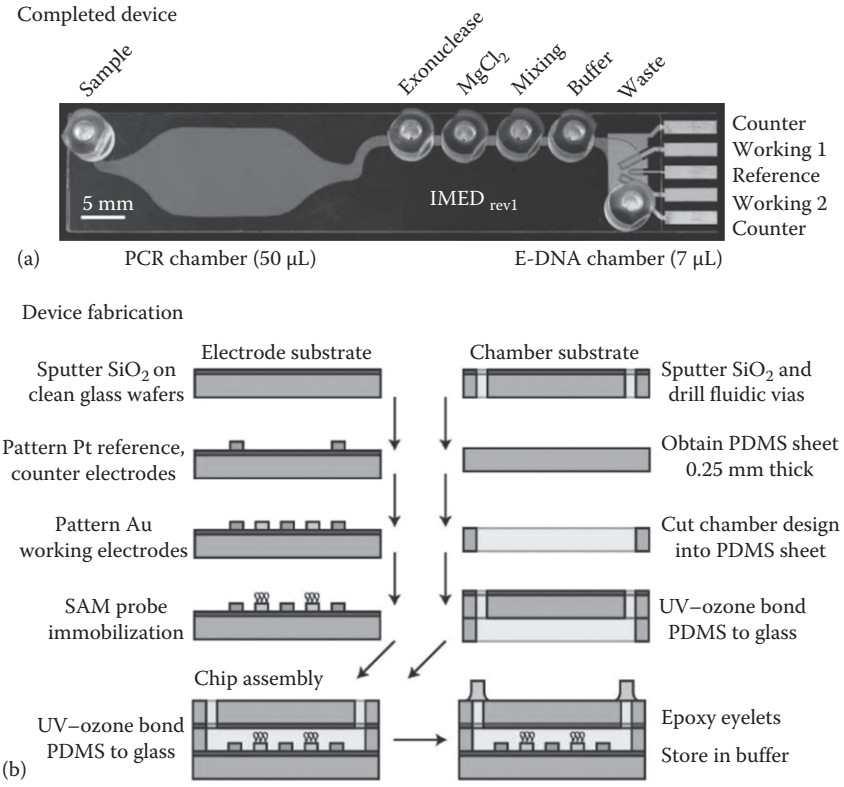

FIGURE 16.7 (a) Architecture and (b) fabrication process of a microfluidic electrochemical DNA sensor. (Reprinted with permission from Ferguson, B.S., Buchsbaum, S.F., Swensen, J.S. et al., Integrated microfluidic electrochemical DNA sensor, *Analytical Chemistry*, 2009, 81, 6503–6508. Copyright 2009 American Chemical Society.)

Fragoso and coworkers reported a system to electrochemically detect breast cancer markers[155] that was realized by high-precision milling of PC sheets forming two distinct sections, a detection zone incorporating an electrode array and a fluid storage zone. The detection zone was divided into separate microfluidic chambers for samples and calibrators, and the fluidic storage zone was split into five reservoirs to store the reagents and sample. The solutions in the separate reservoirs were actuated by applying pressure through a syringe pump and steered to the detection zone via two integrated valves. The detection of protein cancer markers in patient serum samples was demonstrated with detection limits below 10 ng/mL.

Nanogap devices can also be interfaced to fluidic systems. Under typical conditions, the fluidic resistance of the nanochannel is so high that negligible flow takes place within the device; in this case, the fluidics merely serve to bring a sample to the device, but analyte mass transport inside the device remains purely diffusive.[122,163] When sufficient pressure is applied between access points to the detection region, on the other hand, advective flows can develop along the surface of the electrodes. Figure 16.1b shows such a device reported by Mathwig and Lemay[128] in which microfluidic channels created in PDMS were interfaced to a nanochannel containing two separately addressable nanogap transducers. Record-low flow rates at the pL/min level could be measured from analyte time-of-flight measurements between the two electrochemical transducers.

Besides the benefits such as low consumption resulting from miniaturizing the fluidic components, phenomena specific to micro- and nanofluidic systems can also be harnessed to enhance electrochemical response.[1] For example, Wang et al. introduced a preconcentrating device that could be

integrated with an electrochemical detector to study homogeneous enzyme reaction kinetics.[164] The negatively charged enzymes were concentrated via the exclusion-enrichment effect in a nanochannel[165] before being detected electrochemically near the outlet of the channel. In another example, Branagan et al. induced an electroosmotic flow (EOF) through a nanocapillary array membrane to enhance the delivery rate of analyte to annular nanoband electrodes embedded in the membrane.[166] An array of cylindrical nanochannels was created by FIB milling through Au/polymer/Au/polymer membranes and subsequently sandwiched between two axially separated microchannels. The generated EOF enhanced the steady-state current by a factor >10 compared to a comparable structure without convective transport.

It is important to note that many electrochemical micro-/nanofluidic systems still rely on macroscopic reference electrodes that are inserted in a solution reservoir external to the microfluidic system. This is because integrating a reliable, long-lived, and stable microfabricated reference electrode in miniaturized fluidic systems remains a challenge.[167] The main problem is the rapid dissolution of the (small) electrode volume, which leads to short lifetimes. Though pseudoreference electrodes—usually in the form of patterned metal thin films—can be used as a replacement, a true reference is often highly desirable. Analogues to conventional macroscopic liquid-junction reference electrodes have been demonstrated[168–170] in the form of encapsulated thin-film Ag/AgCl electrodes located in a dedicated compartment filled with reference electrolyte of constant Cl^- activity. Incorporating such a device, however, represents significant added complexity of design and fabrication. To form Ag/AgCl layers, an Ag film is normally deposited on an Au or Pt backbone layer in a first step, after which AgCl is formed by passing a current through the Ag layer in a solution with Cl^-.[170] Suzuki et al.[168] demonstrated an approach to fabricate a liquid-junction Ag/AgCl reference electrode using a resin sheet mainly formed by poly(ethylene glycol) as the liquid junction and screen-printed paste prepared from a mixture of KCl and 2-propanol as the electrolyte layer. Poly(vinylpyrrolidone) was added into the electrolyte layer to suppress the dissolution of AgCl, after which the electrode could maintain a stable potential level within ±1 mV for longer than 100 h. In another work Huang et al.[169] demonstrated a gel-coated Ti/Pd/Ag/AgCl electrode in which an agarose-stabilized KCl-gel membrane was introduced to serve both as a polymer-supported solid reference electrolyte and as ionic bridge for the electrode. The variation of the cell potential was less than 2 mV over pH 4–10 and insensitive to changes in the concentration of Cl^- (about 0.02–0.25 mV/pKCl).

16.6 INTEGRATION OF ELECTROCHEMICAL SYSTEMS WITH CMOS ELECTRONICS

By virtue of being inherently electrical in nature, electrochemical sensors are particularly well suited for integration with microelectronics compared to sensors based on other detection principles. While still in relatively early stages of development, such integration could open significant opportunities in applications such as high-throughput screening, point-of-care (POC) diagnosis, and implantable devices with flexibility, scalability, and low cost.

CMOS electronics provide the backbone of most commercial ICs, including microprocessors, microcontrollers, and image sensors. Several CMOS-based potentiostats have been reported. A great deal of flexibility in circuit topology is provided by CMOS, such that it is possible to design integrated circuitry with full potentiostat functionality and a range of operation modes approaching that of tabletop instruments.[171] For particular applications, however, it is often more practical to design more specialized electronics that implement a single electrochemical measurement technique of interest.[172–174] For example, Martin et al.[175] reported a custom integrated system for anodic stripping voltammetry (ASV) in which the detection circuit architecture was cooptimized with the electrode design to minimize parasitics, cancel solution matrix effects, and improve the dynamic range of the system. Alternatively, the relative ease with which addressable arrays can be implemented using CMOS electronics provides an ideal platform for parallelized assays.

This is dramatically illustrated by multiplexed microarrays functionalized with user-dialed probes via local, electronically controlled functionalization[176,177] or DNA synthesis.[178,179] Such systems have been used, for example, for DNA hybridization,[176,179–181] protein arrays,[178] and a range of immunoassays.[177,180]

The electrode materials most commonly employed in electrochemistry span a wide range including gold, platinum, palladium, carbon, graphite, and silver, all of which share the feature of being incompatible with CMOS manufacturing equipment and processes. Electrodes must therefore be formed subsequently to the completion of any CMOS circuitry, in the so-called post-CMOS processing stage. During this stage, high temperatures or intense plasmas that can destroy the circuits must be avoided. Martin et al.[175,182] reported integrated sensing systems for environmental monitoring with two sets of seven Au working electrodes that were selectable via an electronic multiplexer, in addition to two sets of Pt auxiliary electrodes and Ag/AgCl reference electrodes. The post-CMOS processing started with the deposition and lift-off of a Ti/TiN/Ti/Pt layer stack in which the two Ti layers were applied as adhesion promoters and the TiN layer was used as a diffusion barrier between the top-level CMOS metallization and the Pt sensing electrode. Cr/Au and Ti/Ag electrodes were deposited and defined separately in the following steps. Subsequently, the Ag/AgCl reference electrodes were created from the Ag surfaces by submersion of the chip in 1 mM $FeCl_3$ for 2 min.

Another consideration is that it is in general more demanding to package CMOS-based chemical sensors. The chips must be packaged in such a way that the electrical components and interconnects are protected from contact with liquid; otherwise, contaminants from solution may cause the properties of the transistors to drift over time. In specific cases such as protein-based sensors, aggressive electrode cleaning by piranha following organic solutions is required for reliable self-assembly of nanostructured biointerfaces, so the packaging material must withstand this strong corrosiveness. SU-8, polyimide, epoxy, and parylene are the most commonly used passivation material in the reported CMOS electrochemical microsystems.[173] In a microsystem for in situ detection of heavy metals in rainwater,[175] SU-8 was used to form a dam-like structure between the bonding pads and the sensor sites. Packaging was accomplished by fixing the device onto a printed circuit board (PCB) by epoxy, making electrical connections by wire bonding and then encapsulating the wires in a two-coat epoxy process. It was concluded that, using this packaging strategy, the passivation had a lifetime greater than 100 days in saturated salt solutions and the properties of the electronics exhibited only minor drift after soaking in a 100 mM NaCl solution for more than 35 days.

A long-lasting, parylene-packaged, wire-bonded chip that survived a harsh piranha electrode cleaning process was demonstrated by Li et al.[173] The post-CMOS fabrication began with the evaporation and wet etching of Ti/Au to form electrodes, and in the following step, polyimide was spin-coated on the chip and patterned to uncover the electrodes and bonding pads. Afterwards, the chip was wire-bonded to a packaging board and the assembly was coated with 5 μm parylene, following which the parylene was patterned to uncover the electrode sites using RIE in oxygen with a layer of crystal adhesive as the mask. This highlights the strengths of parylene as passivation material for CMOS-integrated bionsensors: high chemical resistance in addition to biocompatibility, biostability, low cytotoxicity, relatively simple chemical vapor deposition methods with low process temperatures, and easy etching in O_2 plasmas.[173]

To achieve a higher level of integration by incorporating microfluidics with CMOS electrochemical sensors and realize a complete lab-on-CMOS system, problems caused by topographical conflicts also need to be solved. The first issue is the size disparity between conventional CMOS chips and microfluidic components, such as channels, valves, and pumps: the former typically occupy a few square millimeters, while microfluidic structures require significantly more area. The other inconvenience is the nonflat morphologies formed through the use of wire bonding or flip-chip bonding, which are the standard packaging techniques employed in the semiconductor industry to form electrical interconnections between CMOS chips and PCBs.

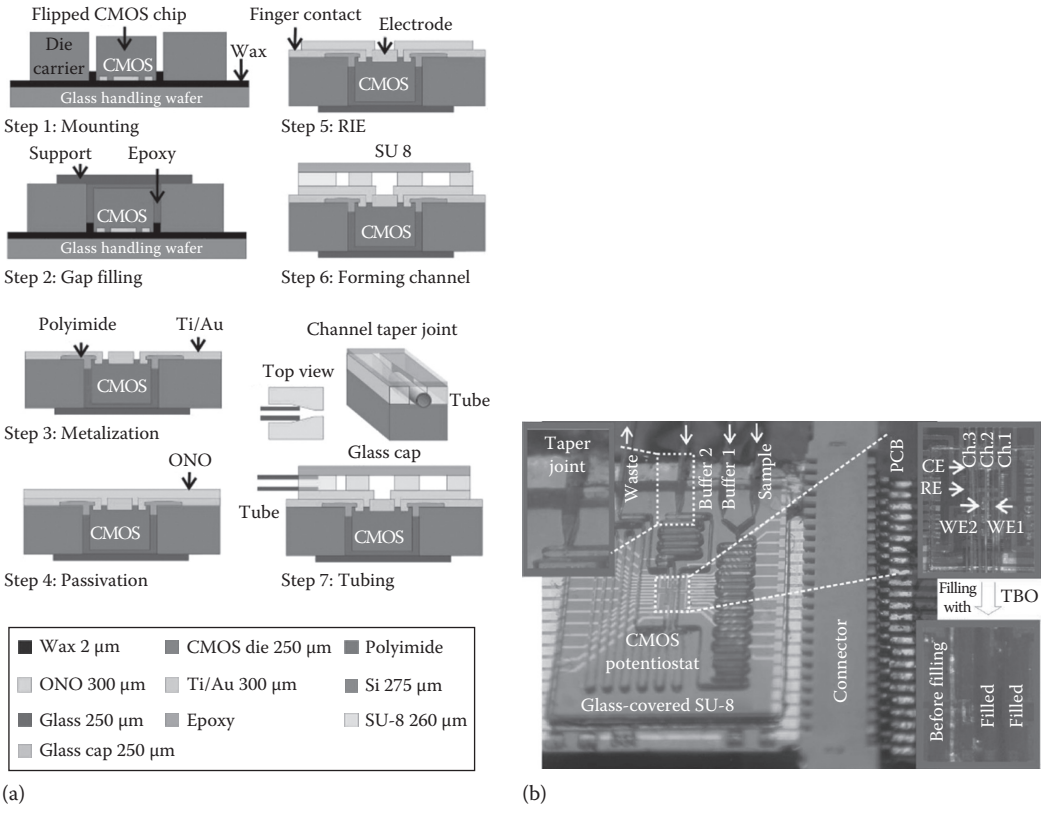

FIGURE 16.8 (a) Schematics of process flow for integrating microfluidics and CMOS electrochemical sensors. (b) The integrated device and schematic of the microfluidic circuits. The insets show (upper left) the taper joint, (upper right) the three microfluidic detection channels across the CMOS potentiostat with on-chip electrodes, and (lower right) the microfluidic channels being filled by TBO. (From Huang, Y. and Mason, A.J., Lab-on-CMOS integration of microfluidics and electrochemical sensors, *Lab Chip*, 13, 3929–3934, 2013. Reproduced by permission of The Royal Society of Chemistry.)

These methods lead to uneven surfaces due to wires protruding out of the surface of the chip, which is itself at a different height than the surrounding board. However, a smooth surface without bumps or steps is usually a necessary starting point to create the microfluidic systems described earlier.

To address these issues, Huang and Mason[183] recently introduced an integration scheme in which the CMOS chip was embedded into a micromachined silicon carrier as the packaging board, as shown in Figure 16.8. Both the CMOS chip and the carrier were first pressed onto a wax-coated glass handling wafer with the front side of the chip facing the handling wafer. The assembly was then placed in a 150°C chamber to allow the wax to melt, evening out the vertical position of the chip and carrier and attaching the chip to the handling wafer. Following this procedure, epoxy was applied to fill the gap between the chip and the carrier. Afterwards, the glass handling wafer was released by softening the wax at 100°C, and the wax remaining on the assembly was cleaned off. Polyimide was then coated onto the surface to smoothen it, metal wires for electrical interconnections were added by thin-film deposition and lithography, and a passivation layer consisting of silicon oxide/nitride/oxide was deposited at 100°C using PECVD. Finally, microfluidic structures with open channels made of SU-8 resist and covered by a glass cap were incorporated. Tubing was inserted laterally into the taper joint located at the sidewall of the SU-8 layer to enable high-density world-to-chip microfluidic interconnections. The integrated

device and schematic of the microfluidic circuits are shown in Figure 16.8b. The simultaneous fluidic and electrical operation of the lab-on-CMOS device was demonstrated by detecting a diluted toluidine blue O (TBO) sample.

A method based on a similar concept was reported by Uddin et al.[184] CMOS chips measuring 3 mm × 3 mm × 260 μm were placed on a resist-coated oxidized silicon wafer and used as the mask to pattern the resist. The pattern was then transferred to the oxide layer and subsequently to the silicon wafer by RIE and DRIE, respectively, so that cavities with approximately the same size as the CMOS chips were generated in this wafer. The wafer was then placed on a handle substrate, and the CMOS chips were placed facedown inside the cavities of the wafer with the help of a flip-chip bonder. Another wafer coated with benzocyclobutene (BCB) was then placed on top of the CMOS chips, and the cavity wafer and the whole stack were placed in a wafer bonding machine with pressure and elevated temperature (250°C). As a result, the CMOS chips and the cavity wafer were bonded to the wafer coated with BCB. In the next step, the handle substrate was removed from the front side of the CMOS chips, and spin-on glass was coated onto the surface to fill in the gap between the chip and the cavity wafer. Access to the contact pads was opened by RIE through the spin-on glass, and metal interconnects between the chip and the carrier were created by evaporation and lift-off. Up to this step, the process was done on the wafer scale, after which the wafer was diced into individual chips. Measurements with the packaged chip showed that the postintegration processing did not affect the CMOS device parameters. A hybrid CMOS/microfluidic system was completed by placing the embedded chip on an acrylic stage and securing it mechanically by fastening an acrylic microfluidic channel on top with screws. A PDMS gasket was used to achieve a tight seal between chip and fluidic channel.

16.7 SUMMARY AND OUTLOOK

This chapter reviewed the development of electrochemical measurement systems fabricated with micromachining technology. This set of techniques enables the systematic downscaling of the dimensions of experimental elements to explore electrochemistry in new regimes and to enhance sensitivity and selectivity in sensor applications. Lithography-based techniques provide the opportunity to build arrays of components with high controllability and repeatability. Additionally, the flexibility to integrate detecting electrodes, microfluidics, and even ICs onto a single chip that includes the functionalities of sensing, fluidic handling, and signal processing potentially creates new opportunities: while not going to replace existing instrumentation for classic measurements, the low costs, low sample and reagent volumes, low power consumptions, and possibility of massive parallelization open the door to new classes of electrochemical analytical methods. One can envision fully integrated microfluidic-based electrochemical measurement systems implemented on top of CMOS electronics to provide high-throughput biomedical analytical platforms, POC diagnostic tools, implantable devices, and portable and disposable food- and environment-monitoring sensors. Although a variety of difficulties remain, such as integration of reference electrode and effective packaging of the compact systems, the rapid pace of development means that such systems could become a practical reality on a relatively short timescale.

REFERENCES

1. Rassaei, L., Singh, P. S., and Lemay, S. G. 2011. Lithography-based nanoelectrochemistry. *Anal. Chem.* 83: 3974–3980.
2. Wightman, R. M. 1981. Microvoltammetric electrodes. *Anal. Chem.* 53: 1125A–1134A.
3. Bard, A. J. and Faulkner, L. R. 2001. *Electrochemical Methods: Fundamentals and Applications*. New York: John Wiley & Sons.
4. Adams, R. N. 1976. Probing brain chemistry with electroanalytical techniques. *Anal. Chem.* 48: 1126A–1138A.

5. Ponchon, J. L., Cespuglio, R., Gonon, F., Jouvet, M., and Pujol, J. F. 1979. Normal pulse polarography with carbon-fiber electrodes for in vitro and in vivo determination of catecholamines. *Anal. Chem.* 51: 1483–1486.
6. McCreery, R. L., Dreiling, R., and Adams, R. N. 1974. Voltammetry in brain-tissue—Quantitative studies of drug interactions. *Brain Res.* 73: 23–33.
7. Adams, R. N. 1978. In vivo electrochemical recording—A new neurophysiological approach. *Trends Neurosci.* 1: 160–163.
8. Thomas, C. A., Jr., Springer, P. A., Loeb, G. E., Berwald-Netter, Y., and Okun, L. M. 1972. A miniature microelectrode array to monitor the bioelectric activity of cultured cells. *Exp. Cell Res.* 74: 61–66.
9. May, G. A., Shamma, S. A., and White, R. L. 1979. Tantalum on sapphire micro-electrode array. *IEEE Trans. Electron Dev.* 26: 1932–1939.
10. Prohaska, O., Olcaytug, F., Womastek, K., and Petsche, H. 1977. Multielectrode for intracortical recordings produced by thin-film technology. *Electroencephalogr. Clin. Neurophysiol.* 42: 421–422.
11. Gross, G. W. 1979. Simultaneous single unit recording in vitro with a photoetched laser deinsulated gold multimicroelectrode surface. *IEEE Trans. Biomed. Eng.* 26: 273–279.
12. Pine, J. 1980. Recording action-potentials from cultured neurons with extracellular micro-circuit electrodes. *J. Neurosci. Methods* 2: 19–31.
13. Thormann, W., Vandenbosch, P., and Bond, A. M. 1985. Voltammetry at linear gold and platinum microelectrode arrays produced by lithographic techniques. *Anal. Chem.* 57: 2764–2770.
14. Kuperstein, M. and Whittington, D. A. 1981. A practical 24 channel microelectrode for neural recording in vivo. *IEEE Trans. Biomed. Eng.* 28: 288–293.
15. Kern, W. and Shaw, J. M. 1971. Electrochemical delineation of tungsten films for microelectronic devices. *J. Electrochem. Soc.* 118: 1699–1704.
16. Siu, W. and Cobbold, R. S. C. 1976. Characteristics of a multicathode polarographic oxygen electrode. *Med. Biol. Eng.* 14: 109–121.
17. Feeney, R. and Kounaves, S. P. 2000. Microfabricated ultramicroelectrode arrays: Developments, advances, and applications in environmental analysis. *Electroanalysis* 12: 677–684.
18. Glass, R. S., Perone, S. P., and Ciarlo, D. R. 1990. Application of information-theory to electroanalytical measurements using a multielement, microelectrode array. *Anal. Chem.* 62: 1914–1918.
19. Compton, R. G., Foord, J. S., and Marken, F. 2003. Electroanalysis at diamond-like and doped-diamond electrodes. *Electroanalysis* 15: 1349–1363.
20. Hu, J. P., Holt, K. B., and Foord, J. S. 2009. Focused ion beam fabrication of boron-doped diamond ultramicroelectrodes. *Anal. Chem.* 81: 5663–5670.
21. Soh, K. L., Kang, W. P., Davidson, J. L. et al. 2004. Diamond-derived microelectrodes array for electrochemical analysis. *Diam. Relat. Mater.* 13: 2009–2015.
22. Simm, A. O., Banks, C. E., Ward-Jones, S. et al. 2005. Boron-doped diamond microdisc arrays: Electrochemical characterisation and their use as a substrate for the production of microelectrode arrays of diverse metals (Ag, Au, Cu) via electrodeposition. *Analyst* 130: 1303–1311.
23. Zoski, C. G., Simjee, N., Guenat, O., and Koudelka-Hep, M. 2004. Addressable microelectrode arrays: Characterization by imaging with scanning electrochemical microscopy. *Anal. Chem.* 76: 62–72.
24. Lin, Z., Takahashi, Y., Kitagawa, Y. et al. 2008. An addressable microelectrode array for electrochemical detection. *Anal. Chem.* 80: 6830–6833.
25. Polsky, R., Harper, J. C., Wheeler, D. R., and Brozik, S. M. 2008. Multifunctional electrode arrays: Towards a universal detection platform. *Electroanalysis* 20: 671–679.
26. Sanchez-Molas, D., Esquivel, J. P., Sabate, N., Munoz, F. X., and del Campo, F. J. 2012. High aspect-ratio, fully conducting gold micropillar array electrodes: Silicon micromachining and electrochemical characterization. *J. Phys. Chem. C* 116: 18831–18846.
27. Wehmeyer, K. R., Deakin, M. R., and Wightman, R. M. 1985. Electroanalytical properties of band electrodes of submicrometer width. *Anal. Chem.* 57: 1913–1916.
28. Arrigan, D. W. M. 2004. Nanoelectrodes, nanoelectrode arrays and their applications. *Analyst* 129: 1157–1165.
29. Huang, X. J., O'Mahony, A. M., and Compton, R. G. 2009. Microelectrode arrays for electrochemistry: Approaches to fabrication. *Small* 5: 776–788.
30. Oja, S. M., Wood, M., and Zhang, B. 2013. Nanoscale electrochemistry. *Anal. Chem.* 85: 473–486.
31. Murray, R. W. 2008. Nanoelectrochemistry: Metal nanoparticles, nanoelectrodes, and nanopores. *Chem. Rev.* 108: 2688–2720.
32. Okazaki, S. 1991. Resolution limits of optical lithography. *J. Vac. Sci. Technol. B* 9: 2829–2833.

33. Zoski, C. G. 2002. Ultramicroelectrodes: Design, fabrication, and characterization. *Electroanalysis* 14: 1041–1051.
34. Cox, J. T. and Zhang, B. 2012. Nanoelectrodes: Recent advances and new directions. *Ann. Rev. Anal. Chem.* 5: 253–272.
35. Nagahara, L. A., Thundat, T., and Lindsay, S. M. 1989. Preparation and characterization of STM tips for electrochemical studies. *Rev. Sci. Instrum.* 60: 3128–3130.
36. Mirkin, M. V., Fan, F. R. F., and Bard, A. J. 1992. Scanning electrochemical microscopy part 13. Evaluation of the tip shapes of nanometer size microelectrodes. *J. Electroanal. Chem.* 328: 47–62.
37. Fan, F. R. F., Kwak, J., and Bard, A. J. 1996. Single molecule electrochemistry. *J. Am. Chem. Soc.* 118: 9669–9675.
38. Sun, P., Zhang, Z. Q., Guo, J. D., and Shao, Y. H. 2001. Fabrication of nanometer-sized electrodes and tips for scanning electrochemical microscopy. *Anal. Chem.* 73: 5346–5351.
39. Slevin, C. J., Gray, N. J., Macpherson, J. V., Webb, M. A., and Unwin, P. R. 1999. Fabrication and characterisation of nanometre-sized platinum electrodes for voltammetric analysis and imaging. *Electrochem. Commun.* 1: 282–288.
40. Conyers, J. L. and White, H. S. 2000. Electrochemical characterization of electrodes with submicrometer dimensions. *Anal. Chem.* 72: 4441–4446.
41. Macpherson, J. V. and Unwin, P. R. 2000. Combined scanning electrochemical-atomic force microscopy. *Anal. Chem.* 72: 276–285.
42. Gray, N. J. and Unwin, P. R. 2000. Simple procedure for the fabrication of silver/silver chloride potentiometric electrodes with micrometre and smaller dimensions: Application to scanning electrochemical microscopy. *Analyst* 125: 889–893.
43. Chen, S. L. and Kucernak, A. 2002. Fabrication of carbon microelectrodes with an effective radius of 1 nm. *Electrochem. Commun.* 4: 80–85.
44. Chen, S. L. and Kucernak, A. 2002. The voltammetric response of nanometer-sized carbon electrodes. *J. Phys. Chem. B* 106: 9396–9404.
45. Abbou, J., Demaille, C., Druet, M., and Moiroux, J. 2002. Fabrication of submicrometer-sized gold electrodes of controlled geometry for scanning electrochemical-atomic force microscopy. *Anal. Chem.* 74: 6355–6363.
46. Watkins, J. J., Chen, J., White, H. S. et al. 2003. Zeptomole voltammetric detection and electron-transfer rate measurements using platinum electrodes of nanometer dimensions. *Anal. Chem.* 75: 3962–3971.
47. Penner, R. M., Heben, M. J., Longin, T. L., and Lewis, N. S. 1990. Fabrication and use of nanometer-sized electrodes in electrochemistry. *Science* 250: 1118–1121.
48. Pendley, B. D. and Abruna, H. D. 1990. Construction of submicrometer voltammetric electrodes. *Anal. Chem.* 62: 782–784.
49. Shao, Y. H., Mirkin, M. V., Fish, G. et al. 1997. Nanometer-sized electrochemical sensors. *Anal. Chem.* 69: 1627–1634.
50. Katemann, B. B. and Schuhmann, T. 2002. Fabrication and characterization of needle-type Pt-disk nanoelectrodes. *Electroanalysis* 14: 22–28.
51. Zhang, B., Zhang, Y. H., and White, H. S. 2004. The nanopore electrode. *Anal. Chem.* 76: 6229–6238.
52. Sun, P. and Mirkin, M. V. 2006. Kinetics of electron-transfer reactions at nanoelectrodes. *Anal. Chem.* 78: 6526–6534.
53. Zhang, B., Galusha, J., Shiozawa, P. G. et al. 2007. Bench-top method for fabricating glass-sealed nanodisk electrodes, glass nanopore electrodes, and glass nanopore membranes of controlled size. *Anal. Chem.* 79: 4778–4787.
54. Thiébaud, P., Beuret, C., de Rooij, N. F., and Koudelka-Hep, M. 2000. Microfabrication of Pt-tip microelectrodes. *Sens. Actuators, B* 70: 51–56.
55. Qiao, Y., Chen, J., Guo, X. L. et al. 2005. Fabrication of nanoelectrodes for neurophysiology: Cathodic electrophoretic paint insulation and focused ion beam milling. *Nanotechnology* 16: 1598–1602.
56. Menke, E. J., Thompson, M. A., Xiang, C., Yang, L. C., and Penner, R. M. 2006. Lithographically patterned nanowire electrodeposition. *Nat. Mater.* 5: 914–919.
57. Yang, F., Taggart, D. K., and Penner, R. M. 2009. Fast, sensitive hydrogen gas detection using single palladium nanowires that resist fracture. *Nano Lett.* 9: 2177–2182.
58. Hujdic, J. E., Sargisian, A. P., Shao, J. R., Ye, T., and Menke, E. J. 2011. High-density gold nanowire arrays by lithographically patterned nanowire electrodeposition. *Nanoscale* 3: 2697–2699.
59. Heo, J. I., Shim, D. S., Teixidor, G. T. et al. 2011. Carbon interdigitated array nanoelectrodes for electrochemical applications. *J. Electrochem. Soc.* 158: J76–J80.

60. Varnell, G. L., Spicer, D. F., and Rodger, A. C. 1973. E-beam writing techniques for semiconductor-device fabrication. *J. Vac. Sci. Technol.* 10: 1048–1051.
61. Finot, E., Bourillot, E., Meunier-Prest, R. et al. 2003. Performance of interdigitated nanoelectrodes for electrochemical DNA biosensor. *Ultramicroscopy* 97: 441–449.
62. Sandison, M. E. and Cooper, J. M. 2006. Nanofabrication of electrode arrays by electron-beam and nano-imprint lithographies. *Lab Chip* 6: 1020–1025.
63. Naka, K., Hayashi, H., Senda, M., Shiraishi, H., and Konishi, S. 2007. Effect of nano stripe carbonized-polymer electrode on high S/N ratio in electrochemical detection. *Proceedings of the IEEE Twentieth Annual International Conference on Micro Electro Mechanical Systems*, Hyogo, Japan 1/2: 374–377.
64. Hoeben, F. J. M., Meijer, F. S., Dekker, C. et al. 2008. Toward single-enzyme molecule electrochemistry: [NiFe]-hydrogenase protein film voltammetry at nanoelectrodes. *ACS Nano* 2: 2497–2504.
65. Moretto, L. M., Tormen, M., De Leo, M., Carpentiero, A., and Ugo, P. 2011. Polycarbonate-based ordered arrays of electrochemical nanoelectrodes obtained by e-beam lithography. *Nanotechnology* 22: 185305.
66. Dawson, K., Wahl, A., Murphy, R., and O'Riordan, A. 2012. Electroanalysis at single gold nanowire electrodes. *J. Phys. Chem. C* 116: 14665–14673.
67. Kleijn, S. E. F., Yanson, A. I., and Koper, M. T. M. 2012. Electrochemical characterization of nano-sized gold electrodes fabricated by nano-lithography. *J. Electroanal. Chem.* 666: 19–24.
68. Niwa, O., Morita, M., and Tabei, H. 1990. Electrochemical-behavior of reversible redox species at interdigitated array electrodes with different geometries—consideration of redox cycling and collection efficiency. *Anal. Chem.* 62: 447–452.
69. Lanyon, Y. H. and Arrigan, D. W. M. 2007. Recessed nanoband electrodes fabricated by focused ion beam milling. *Sens. Actuators B* 121: 341–347.
70. Lanyon, Y. H., De Marzi, G., Watson, Y. E. et al. 2007. Fabrication of nanopore array electrodes by focused ion beam milling. *Anal. Chem.* 79: 3048–3055.
71. Rauf, S., Shiddiky, M. J. A., Asthana, A., and Dimitrov, K. 2012. Fabrication and characterization of gold nanohole electrode arrays. *Sens. Actuators B* 173: 491–496.
72. Menon, V. P. and Martin, C. R. 1995. Fabrication and evaluation of nanoelectrode ensembles. *Anal. Chem.* 67: 1920–1928.
73. Penner, R. M. and Martin, C. R. 1987. Preparation and electrochemical characterization of ultramicroelectrode ensembles. *Anal. Chem.* 59: 2625–2630.
74. Lemay, S. G., van den Broek, D. M., Storm, A. J. et al. 2005. Lithographically fabricated nanopore-based electrodes for electrochemistry. *Anal. Chem.* 77: 1911–1915.
75. Krapf, D., Wu, M. Y., Smeets, R. M. M. et al. 2006. Fabrication and characterization of nanopore-based electrodes with radii down to 2 nm. *Nano Lett.* 6: 105–109.
76. Yang, M., Qu, F., Lu, Y. et al. 2006. Platinum nanowire nanoelectrode array for the fabrication of biosensors. *Biomaterials* 27: 5944–5950.
77. Chou, S. Y., Krauss, P. R., and Renstrom, P. J. 1996. Imprint lithography with 25-nanometer resolution. *Science* 272: 85–87.
78. Beck, M., Persson, F., Carlberg, P. et al. 2004. Nanoelectrochemical transducers for (bio-) chemical sensor applications fabricated by nanoimprint lithography. *Microelectron. Eng.* 73–4: 837–842.
79. Huang, C. W. and Lu, M. S. C. 2011. Electrochemical detection of the neurotransmitter dopamine by nanoimprinted interdigitated electrodes and a CMOS circuit with enhanced collection efficiency. *IEEE Sens. J.* 11: 1826–1831.
80. Haynes, C. L. and Van Duyne, R. P. 2001. Nanosphere lithography: A versatile nanofabrication tool for studies of size-dependent nanoparticle optics. *J. Phys. Chem. B* 105: 5599–5611.
81. Valsesia, A., Lisboa, P., Colpo, P., and Rossi, F. 2006. Fabrication of polypyrrole-based nanoelectrode arrays by colloidal lithography. *Anal. Chem.* 78: 7588–7591.
82. Lohmuller, T., Muller, U., Breisch, S. et al. 2008. Nano-porous electrode systems by colloidal lithography for sensitive electrochemical detection: Fabrication technology and properties. *J. Micromech. Microeng.* 18: 115011.
83. Hees, J., Hoffmann, R., Kriele, A. et al. 2011. Nanocrystalline diamond nanoelectrode arrays and ensembles. *ACS Nano* 5: 3339–3346.
84. Ma, C., Contento, N. M., Gibson, L. R., 2nd, and Bohn, P. W. 2013. Recessed ring-disk nanoelectrode arrays integrated in nanofluidic structures for selective electrochemical detection. *Anal. Chem.* 85: 9882–9888.
85. Morris, R. B., Franta, D. J., and White, H. S. 1987. Electrochemistry at Pt band electrodes of width approaching molecular dimensions—Breakdown of transport-equations at very small electrodes. *J. Phys. Chem.* 91: 3559–3564.

86. Dumitrescu, I., Unwin, P. R., and Macpherson, J. V. 2009. Electrochemistry at carbon nanotubes: Perspective and issues. *Chem. Commun.* 7: 6886–6901.
87. Dumitrescu, I., Unwin, P. R., Wilson, N. R., and Macpherson, J. V. 2008. Single-walled carbon nanotube network ultramicroelectrodes. *Anal. Chem.* 80: 3598–3605.
88. Dumitrescu, I., Edgeworth, J. P., Unwin, P. R., and Macpherson, J. V. 2009. Ultrathin carbon nanotube mat electrodes for enhanced amperometric detection. *Adv. Mater.* 21: 3105–3109.
89. Heller, I., Kong, J., Heering, H. A. et al. 2005. Individual single-walled carbon nanotubes as nanoelectrodes for electrochemistry. *Nano Lett.* 5: 137–142.
90. Quinn, B. M. and Lemay, S. G. 2006. Single-walled carbon nanotubes as templates and interconnects for nanoelectrodes. *Adv. Mater.* 18: 855–859.
91. Day, T. M., Unwin, P. R., Wilson, N. R., and Macpherson, J. V. 2005. Electrochemical templating of metal nanoparticles and nanowires on single-walled carbon nanotube networks. *J. Am. Chem. Soc.* 127: 10639–10647.
92. Quinn, B. M., Dekker, C., and Lemay, S. G. 2005. Electrodeposition of noble metal nanoparticles on carbon nanotubes. *J. Am. Chem. Soc.* 127: 6146–6147.
93. Dawson, K., Strutwolf, J., Rodgers, K. P. et al. 2011. Single nanoskived nanowires for electrochemical applications. *Anal. Chem.* 83: 5535–5540.
94. Xu, Q., Rioux, R. M., Dickey, M. D., and Whitesides, G. M. 2008. Nanoskiving: A new method to produce arrays of nanostructures. *Acc. Chem. Res.* 41: 1566–1577.
95. Campbell, J. K., Sun, L., and Crooks, R. M. 1999. Electrochemistry using single carbon nanotubes. *J. Am. Chem. Soc.* 121: 3779–3780.
96. Guillorn, M. A., McKnight, T. E., Melechko, A. et al. 2002. Individually addressable vertically aligned carbon nanofiber-based electrochemical probes. *J. Appl. Phys.* 91: 3824–3828.
97. Mai, L., Dong, Y., Xu, L., and Han, C. 2010. Single nanowire electrochemical devices. *Nano Lett.* 10: 4273–4278.
98. Zhao, M., Huang, J., Zhou, Y. et al. 2013. A single mesoporous ZnO/chitosan hybrid nanostructure for a novel free nanoprobe type biosensor. *Biosens. Bioelectron.* 43: 226–230.
99. Percival, S. J. and Zhang, B. 2013. Electrocatalytic reduction of oxygen at single platinum nanowires. *J. Phys. Chem. C* 117: 13928–13935.
100. Kranz, C., Friedbacher, G., Mizaikoff, B. et al. 2001. Integrating an ultramicroelectrode in an AFM cantilever: Combined technology for enhanced information. *Anal. Chem.* 73: 2491–2500.
101. Lugstein, A., Bertagnolli, E., Kranz, C., and Mizaikoff, B. 2002. Fabrication of a ring nanoelectrode in an AFM tip: Novel approach towards simultaneous electrochemical and topographical imaging. *Surf. Interface Anal.* 33: 146–150.
102. Burt, D. P., Wilson, N. R., Weaver, J. M. R., Dobson, P. S., and Macpherson, J. V. 2005. Nanowire probes for high resolution combined scanning electrochemical microscopy—Atomic force microscopy. *Nano Lett.* 5: 639–643.
103. Bai, S. J., Fabian, T., Prinz, F. B., and Fasching, R. J. 2008. Nanoscale probe system for cell-organelle analysis. *Sens. Actuators B* 130: 249–257.
104. Smirnov, W., Kriele, A., Hoffmann, R. et al. 2011. Diamond-modified AFM probes: From diamond nanowires to atomic force microscopy-integrated boron-doped diamond electrodes. *Anal. Chem.* 83: 4936–4941.
105. Sanderson, D. G. and Anderson, L. B. 1985. Filar electrodes—steady-state currents and spectroelectrochemistry at twin interdigitated electrodes. *Anal. Chem.* 57: 2388–2393.
106. Aoki, K., Morita, M., Niwa, O., and Tabei, H. 1988. Quantitative-analysis of reversible diffusion-controlled currents of redox soluble species at interdigitated array electrodes under steady-state conditions. *J. Electroanal. Chem.* 256: 269–282.
107. Niwa, O., Xu, Y., Halsall, H. B., and Heineman, W. R. 1993. Small-volume voltammetric detection of 4-Aminophenol with interdigitated array electrodes and its application to electrochemical enzyme-immunoassay. *Anal. Chem.* 65: 1559–1563.
108. Dam, V. A. T., Olthuis, W., and van den Berg, A. 2007. Redox cycling with facing interdigitated array electrodes as a method for selective detection of redox species. *Analyst* 132: 365–370.
109. Goluch, E. D., Wolfrum, B., Singh, P. S., Zevenbergen, M. A. G., and Lemay, S. G. 2009. Redox cycling in nanofluidic channels using interdigitated electrodes. *Anal. Bioanal. Chem.* 394: 447–456.
110. Ino, K., Saito, W., Koide, M. et al. 2011. Addressable electrode array device with IDA electrodes for high-throughput detection. *Lab Chip* 11: 385–388.
111. Ino, K., Nishijo, T., Arai, T. et al. 2012. Local redox-cycling-based electrochemical chip device with deep microwells for evaluation of embryoid bodies. *Angew. Chem. Int. Ed.* 51: 6648–6652.

112. Henry, C. S. and Fritsch, I. 1999. Microcavities containing individually addressable recessed microdisk and tubular nanoband electrodes. *J. Electrochem. Soc.* 146: 3367–3373.
113. Vandaveer, W. R., Woodward, D. J., and Fritsch, I. 2003. Redox cycling measurements of a model compound and dopamine in ultrasmall volumes with a self-contained microcavity device. *Electrochim. Acta* 48: 3341–3348.
114. Neugebauer, S., Muller, U., Lohmuller, T. et al. 2006. Characterization of nanopore electrode structures as basis for amplified electrochemical assays. *Electroanalysis* 18: 1929–1936.
115. Menshykau, D., O'Mahony, A. M., del Campo, F. J., Munoz, F. X., and Compton, R. G. 2009. Microarrays of ring-recessed disk electrodes in transient generator-collector mode: Theory and experiment. *Anal. Chem.* 81: 9372–9382.
116. Menshykau, D., del Campo, F. J., Munoz, F. X., and Compton, R. G. 2009. Current collection efficiency of micro- and nano-ring-recessed disk electrodes and of arrays of these electrodes. *Sens. Actuators B* 138: 362–367.
117. Ma, C. X., Contento, N. M., Gibson, L. R., and Bohn, P. W. 2013. Redox cycling in nanoscale-recessed ring-disk electrode arrays for enhanced electrochemical sensitivity. *ACS Nano* 7: 5483–5490.
118. Zevenbergen, M. A. G., Krapf, D., Zuiddam, M. R., and Lemay, S. G. 2007. Mesoscopic concentration fluctuations in a fluidic nanocavity detected by redox cycling. *Nano Lett.* 7: 384–388.
119. Wolfrum, B., Zevenbergen, M., and Lemay, S. 2008. Nanofluidic redox cycling amplification for the selective detection of catechol. *Anal. Chem.* 80: 972–977.
120. Zevenbergen, M. A. G., Wolfrum, B. L., Goluch, E. D., Singh, P. S., and Lemay, S. G. 2009. Fast electron-transfer kinetics probed in nanofluidic channels. *J. Am. Chem. Soc.* 131: 11471–11477.
121. Zevenbergen, M. A. G., Singh, P. S., Goluch, E. D., Wolfrum, B. L., and Lemay, S. G. 2009. Electrochemical correlation spectroscopy in nanofluidic cavities. *Anal. Chem.* 81: 8203–8212.
122. Katelhon, E., Hofmann, B., Lemay, S. G. et al. 2010. Nanocavity redox cycling sensors for the detection of dopamine fluctuations in microfluidic gradients. *Anal. Chem.* 82: 8502–8509.
123. Zevenbergen, M. A. G., Singh, P. S., Goluch, E. D., Wolfrum, B. L., and Lemay, S. G. 2011. Stochastic sensing of single molecules in a nanofluidic electrochemical device. *Nano Lett.* 11: 2881–2886.
124. Kim, J. H., Moon, H., Yoo, S., and Choi, Y. K. 2011. Nanogap electrode fabrication for a nanoscale device by volume-expanding electrochemical synthesis. *Small* 7: 2210–2216.
125. Kang, S., Mathwig, K., and Lemay, S. G. 2012. Response time of nanofluidic electrochemical sensors. *Lab Chip* 12: 1262–1267.
126. Mathwig, K., Mampallil, D., Kang, S., and Lemay, S. G. 2012. Electrical cross-correlation spectroscopy: Measuring picoliter-per-minute flows in nanochannels. *Phys. Rev. Lett.* 109: 118302.
127. Kang, S., Nieuwenhuis, A. F., Mathwig, K., Mampallil, D., and Lemay, S. G. 2013. Electrochemical single-molecule detection in aqueous solution using self-aligned nanogap transducers. *ACS Nano* 7: 10931–10937.
128. Mathwig, K. and Lemay, S. G. 2013. Pushing the limits of electrical detection of ultralow flows in nanofluidic channels. *Micromachines* 4: 138–148.
129. Mampallil, D., Mathwig, K., Kang, S., and Lemay, S. G. 2013. Redox couples with unequal diffusion coefficients: Effect on redox cycling. *Anal. Chem.* 85: 6053–6058.
130. McCarty, G. S., Moody, B., and Zachek, M. K. 2010. Enhancing electrochemical detection by scaling solid state nanogaps. *J. Electroanal. Chem.* 643: 9–14.
131. Van Gerwen, P., Laureyn, W., Laureys, W. et al. 1998. Nanoscaled interdigitated electrode arrays for biochemical sensors. *Sens. Actuators B* 49: 73–80.
132. Yang, L. J., Li, Y. B., and Erf, G. F. 2004. Interdigitated array microelectrode-based electrochemical impedance immunosensor for detection of *Escherichia coli* O157: H7. *Anal. Chem.* 76: 1107–1113.
133. Heo, J. I., Lim, Y., and Shin, H. 2013. The effect of channel height and electrode aspect ratio on redox cycling at carbon interdigitated array nanoelectrodes confined in a microchannel. *Analyst* 138: 6404–6411.
134. Albery, W. J. H. and Hitchman, M. L. 1971. *Ring-Disc Electrodes*. Lodon, U.K.: Oxford University Press.
135. Zhao, G., Giolando, D. M., and Kirchhoff, J. R. 1995. Carbon ring disk ultramicroelectrodes. *Anal. Chem.* 67: 1491–1495.
136. Liljeroth, P., Johans, C., Slevin, C. J., Quinn, B. M., and Kontturi, K. 2002. Disk-generation/ring-collection scanning electrochemical microscopy: Theory and application. *Anal. Chem.* 74: 1972–1978.
137. Yakushenko, A., Kaetelhoen, E., and Wolfrum, B. 2013. Parallel on-chip analysis of single vesicle neurotransmitter release. *Anal. Chem.* 85: 5483–5490.

138. Reed, M. A., Zhou, C., Muller, C. J., Burgin, T. P., and Tour, J. M. 1997. Conductance of a molecular junction. *Science* 278: 252–254.
139. Joachim, C., Gimzewski, J. K., and Aviram, A. 2000. Electronics using hybrid-molecular and mono-molecular devices. *Nature* 408: 541–548.
140. Akkerman, H. B., Blom, P. W. M., de Leeuw, D. M., and de Boer, B. 2006. Towards molecular electronics with large-area molecular junctions. *Nature* 441: 69–72.
141. Manz, A., Fettinger, J. C., Verpoorte, E. et al. 1991. Micromachining of monocrystalline silicon and glass for chemical-analysis systems—A look into next century technology or just a fashionable craze. *Trends Anal. Chem.* 10: 144–149.
142. Kovacs, G. T. A., Petersen, K., and Albin, M. 1996. Silicon micromachining—Sensors to systems. *Anal. Chem.* 68: A407–A412.
143. Erickson, D. and Li, D. Q. 2004. Integrated microfluidic devices. *Anal. Chim. Acta* 507: 11–26.
144. Lin, Y. H., Wu, H., Timchalk, C. A., and Thrall, K. D. 2002. Integrated microfluidics/electrochemical sensor system for monitoring of environmental exposures to toxic chemicals. *Abstr. Pap. Am. Chem. Soc.* 223: U77.
145. Wang, J. 2002. Electrochemical detection for microscale analytical systems: A review. *Talanta* 56: 223–231.
146. Rossier, J., Reymond, F., and Michel, P. E. 2002. Polymer microfluidic chips for electrochemical and biochemical analyses. *Electrophoresis* 23: 858–867.
147. Wang, J. 2005. Electrochemical detection for capillary electrophoresis microchips: A review. *Electroanalysis* 17: 1133–1140.
148. Bange, A., Halsall, H. B., and Heineman, W. R. 2005. Microfluidic immunosensor systems. *Biosens. Bioelectron.* 20: 2488–2503.
149. Goral, V. N., Zaytseva, N. V., and Baeumner, A. J. 2006. Electrochemical microfluidic biosensor for the detection of nucleic acid sequences. *Lab Chip* 6: 414–421.
150. Sadik, O. A., Aluoch, A. O., and Zhou, A. L. 2009. Status of biomolecular recognition using electrochemical techniques. *Biosens. Bioelectron.* 24: 2749–2765.
151. Swensen, J. S., Xiao, Y., Ferguson, B. S. et al. 2009. Continuous, real-time monitoring of cocaine in undiluted blood serum via a microfluidic, electrochemical aptamer-based sensor. *J. Am. Chem. Soc.* 131: 4262–4266.
152. Kraly, J. R., Holcomb, R. E., Guan, Q., and Henry, C. S. 2009. Review: Microfluidic applications in metabolomics and metabolic profiling. *Anal. Chim. Acta* 653: 23–35.
153. Dungchai, W., Chailapakul, O., and Henry, C. S. 2009. Electrochemical detection for paper-based microfluidics. *Anal. Chem.* 81: 5821–5826.
154. Jang, A., Zou, Z. W., Lee, K. K., Ahn, C. H., and Bishop, P. L. 2011. State-of-the-art lab chip sensors for environmental water monitoring. *Meas. Sci. Technol.* 22: 032001.
155. Fragoso, A., Latta, D., Laboria, N. et al. 2011. Integrated microfluidic platform for the electrochemical detection of breast cancer markers in patient serum samples. *Lab Chip* 11: 625–631.
156. Hebert, N. E., Kuhr, W. G. and Brazill, S. A. 2002. Microchip capillary electrophoresis coupled to sinusoidal voltammetry for the detection of native carbohydrates. *Electrophoresis* 23: 3750–3759.
157. Zhan, W., Alvarez, J., and Crooks, R. M. 2003. A two-channel microfluidic sensor that uses anodic electrogenerated chemiluminescence as a photonic reporter of cathodic redox reactions. *Anal. Chem.* 75: 313–318.
158. Zou, Z. W., Kai, J. H., Rust, M. J., Han, J., and Ahn, C. H. 2007. Functionalized nano interdigitated electrodes arrays on polymer with integrated microfluidics for direct bio-affinity sensing using impedimetric measurement. *Sens. Actuators A* 136: 518–526.
159. Lorenz, H., Despont, M., Fahrni, N. et al. 1997. SU-8: A low-cost negative resist for MEMS. *J. Micromech. Microeng.* 7: 121–124.
160. Castano-Alvarez, M., Fernandez-Abedul, M. T., Costa-Garcia, A. et al. 2009. Fabrication of SU-8 based microchip electrophoresis with integrated electrochemical detection for neurotransmitters. *Talanta* 80: 24–30.
161. Liu, X., Barizuddin, S., Shin, W. et al. 2011. Microwell device for targeting single cells to electrochemical microelectrodes for high-throughput amperometric detection of quantal exocytosis. *Anal. Chem.* 83: 2445–2451.
162. Ferguson, B. S., Buchsbaum, S. F., Swensen, J. S. et al. 2009. Integrated microfluidic electrochemical DNA sensor. *Anal. Chem.* 81: 6503–6508.
163. Rassaei, L., Mathwig, K., Goluch, E. D., and Lemay, S. G. 2012. Hydrodynamic voltammetry with nanogap electrodes. *J. Phys. Chem. C* 116: 10913–10916.

164. Wang, C., Li, S. J., Wu, Z. Q. et al. 2010. Study on the kinetics of homogeneous enzyme reactions in a micro/nanofluidics device. *Lab Chip* 10: 639–646.
165. Plecis, A., Schoch, R. B., and Renaud, P. 2005. Ionic transport phenomena in nanofluidics: Experimental and theoretical study of the exclusion-enrichment effect on a chip. *Nano Lett.* 5: 1147–1155.
166. Branagan, S. P., Contento, N. M., and Bohn, P. W. 2012. Enhanced mass transport of electroactive species to annular nanoband electrodes embedded in nanocapillary array membranes. *J. Am. Chem. Soc.* 134: 8617–8624.
167. Shinwari, M. W., Zhitomirsky, D., Deen, I. A. et al. 2010. Microfabricated reference electrodes and their biosensing applications. *Sensors* 10: 1679–1715.
168. Suzuki, H., Shiroishi, H., Sasaki, S., and Karube, I. 1999. Microfabricated liquid junction Ag/AgCl reference electrode and its application to a one-chip potentiometric sensor. *Anal. Chem.* 71: 5069–5075.
169. Huang, I. Y., Huang, R. S., and Lo, L. H. 2003. Improvement of integrated Ag/AgCl thin-film electrodes by KCl-gel coating for ISFET applications. *Sens. Actuators B* 94: 53–64.
170. Zhou, J. H., Ren, K. N., Zheng, Y. Z. et al. 2010. Fabrication of a microfluidic Ag/AgCl reference electrode and its application for portable and disposable electrochemical microchips. *Electrophoresis* 31: 3083–3089.
171. Hassibi, A. and Lee, T. H. 2006. A programmable 0.18-mu m CMOS electrochemical sensor microarray for biomolecular detection. *IEEE Sens. J.* 6: 1380–1388.
172. Zhu, X. S. and Ahn, C. H. 2006. On-chip electrochemical analysis system using nanoelectrodes and bioelectronic CMOS chip. *IEEE Sens. J.* 6: 1280–1286.
173. Li, L., Liu, X. W., Qureshi, W. A., and Mason, A. J. 2011. CMOS amperometric instrumentation and packaging for biosensor array applications. *IEEE Trans. Biomed. Circuits Syst.* 5: 439–448.
174. Huang, Y., Liu, Y., Hassler, B. L., Worden, R. M., and Mason, A. J. 2013. A protein-based electrochemical biosensor array platform for integrated microsystems. *IEEE Trans. Biomed. Circuits Syst.* 7: 43–51.
175. Martin, S. M., Gebara, F. H., Larivee, B. J., and Brown, R. B. 2005. A CMOS-integrated microinstrument for trace detection of heavy metals. *IEEE J. Solid-State Circ.* 40: 2777–2786.
176. Swanson, P., Gelbart, R., Atlas, E. et al. 2000. A fully multiplexed CMOS biochip for DNA analysis. *Sens. Actuators B* 64: 22–30.
177. Dill, K., Montgomery, D. D., Wang, W., and Tsai, J. C. 2001. Antigen detection using microelectrode array microchips. *Anal. Chim. Acta.* 444: 69–78.
178. Oleinikov, A. V., Gray, M. D., Zhao, J. et al. 2003. Self-assembling protein arrays using electronic semiconductor microchips and in vitro translation. *J. Proteome Res.* 2: 313–319.
179. Maurer, K., Cooper, J., Caraballo, M. et al. 2006. Electrochemically generated acid and its containment to 100 micron reaction areas for the production of DNA microarrays. *PLoS ONE* 1: e34.
180. Dill, K., Montgomery, D. D., Ghindilis, A. L., and Schwarzkopf, K. R. 2004. Immunoassays and sequence-specific DNA detection on a microchip using enzyme amplified electrochemical detection. *J. Biochem. Biophys. Methods* 59: 181–187.
181. Maurer, K., Yazvenko, N., Wilmoth, J. et al. 2010. Use of a multiplexed CMOS microarray to optimize and compare oligonucleotide binding to DNA probes synthesized or immobilized on individual electrodes. *Sensors* 10: 7371–7385.
182. Martin, S. M., Strong, T. D., and Brown, R. B. 2004. Design, implementation, and verification of a CMOS-integrated chemical sensor system. *Proceedings. 2004 International Conference on MEMS, NANO and Smart Systems, 2004*, pp. 379–385.
183. Huang, Y. and Mason, A. J. 2013. Lab-on-CMOS integration of microfluidics and electrochemical sensors. *Lab Chip* 13: 3929–3934.
184. Uddin, A., Milaninia, K., Chen, C. H., and Theogarajan, L. 2011. Wafer scale integration of CMOS chips for biomedical applications via self-aligned masking. *IEEE Trans. Compon., Packag., Manuf. Technol.* 1: 1996–2004.
185. Ueno, K., Hayashida, M., Ye, J., and Misawa, H. 2005. Fabrication and electrochemical characterization of interdigitated nanoelectrode arrays. *Electrochemistry Communications* 7: 161–165.